



**HAL**  
open science

## Highlighting the “structure–reactivity” relationship and the impact on the kinetics for the autoxidation reaction of hydrocarbons

Soraya Aminane, Mickaël Sicard, Yanis Melliti, Bruno Raepsaet, Lorette Sicard, Frédéric Ser

### ► To cite this version:

Soraya Aminane, Mickaël Sicard, Yanis Melliti, Bruno Raepsaet, Lorette Sicard, et al.. Highlighting the “structure–reactivity” relationship and the impact on the kinetics for the autoxidation reaction of hydrocarbons. *Fuel*, 2024, 370, pp.131748. 10.1016/j.fuel.2024.131748 . hal-04585306

**HAL Id: hal-04585306**

**<https://u-paris.hal.science/hal-04585306v1>**

Submitted on 25 Sep 2024

**HAL** is a multi-disciplinary open access archive for the deposit and dissemination of scientific research documents, whether they are published or not. The documents may come from teaching and research institutions in France or abroad, or from public or private research centers.

L'archive ouverte pluridisciplinaire **HAL**, est destinée au dépôt et à la diffusion de documents scientifiques de niveau recherche, publiés ou non, émanant des établissements d'enseignement et de recherche français ou étrangers, des laboratoires publics ou privés.

1 Highlighting the “structure-reactivity” relationship  
2 and the impact on the kinetics for the autoxidation  
3 reaction of hydrocarbons

4 *Soraya Aminane*<sup>a</sup>, *Mickaël Sicard*<sup>\*,a</sup>, *Yanis Melliti*<sup>a</sup>, *Bruno Raepsaet*<sup>a</sup>, *Lorette Sicard*<sup>b</sup>,  
5 *Frédéric Ser*<sup>a</sup>

6 <sup>a</sup>DMPE, ONERA, Université Paris Saclay, F-91123, Palaiseau, France,

7 <sup>b</sup> Université Paris Cité, CNRS, ITODYS, F-75013 Paris, France

8 \*E-mail: mickael.sicard@onera.fr

9 **KEY WORDS:** autoxidation, PetroOXY, model molecule, structure-reactivity, kinetics

10 **ABSTRACT**

11 The interactions between heteroatomic species and the hydrocarbons present in Jet A-1 make the  
12 determination of degradation mechanisms difficult to elucidate and predict. This study aims to  
13 investigate the reaction mechanisms and kinetics of hydrocarbon molecules constituting jet fuel,  
14 excluding molecules with polar species. Five model hydrocarbons were selected (n-dodecane and  
15 its isomeric mixture, n-butylcyclohexane, 1,2,4-trimethylbenzene and 1-methylnaphthalene) and  
16 individually subjected to oxidation using the PetroOXY apparatus, focusing on the onset of  
17 autoxidation ( $\Delta P/P_{\max} = 2$  to 10 %). For the first time, an experimental protocol has been developed  
18 for the monitoring of gas and liquid phase reagent consumption and the identification and  
19 quantification of oxidation products formed in these phases. The results showed that oxygen  
20 consumption was always higher than that of the initial hydrocarbons, suggesting competitive  
21 reactions, with alkanes consuming more oxygen than aromatic molecules, as confirmed by  
22 induction periods (IP), demonstrating the different reactivity depending on the structure of the

23 oxidized hydrocarbon molecule. A relationship between initial hydrocarbon structure and the type  
24 and number of carbon atoms in oxidation products was also demonstrated. A gel, probably a  
25 precursor deposit, was obtained after oxidation of the molecules, indicating a potential  
26 precipitation of polar species due to the difference in polarity with the hydrocarbon molecules. In  
27 addition, the overall kinetic and hydroperoxide dissociation constants of the reaction could be  
28 calculated from tests carried out at different temperatures (140, 150 and 160 °C). The Arrhenius  
29 parameter values were higher for alkanes than for aromatics, confirming the structure-reactivity  
30 relationship of hydrocarbons. A strong correlation between the Arrhenius parameters and the  
31 nature of the oxidized molecules was also demonstrated. This experimental study will be useful  
32 for the calibration of future kinetic models according to the chemical structure of the oxidized  
33 hydrocarbons and for the assessment of thermal stability behavior of 100 % Synthetic Alternative  
34 Fuels (SAF).

## 35 **ABBREVIATIONS**

ACN	Acetonitrile
ATR	Attenuated Total Reflectance
DFT	Density Functional Theory
FID	Flame Ionization Detector
FTIR	Fourier Transformed Infra-Red
GC	Gas Chromatography
GC-MS	Gas Chromatography-Mass Spectrometry
IP	Induction Period
k''	Kinetics constant of the hydroperoxide dissociation reaction
K	Global kinetic constant of autoxidation reaction
KPH	Ketohydroperoxide
μ-GC	Micro-Gas Chromatography
PV	Peroxide Value
ROOH	Hydroperoxide
SAF	Synthetic Alternative fuel
SMORS	Soluble Macromolecular Oxidation Reactive Species
TAN	Total Acid Number
TCD	Thermal Conductivity Detectors

THF	Tetrahydrofuran
TPP	Triphenylphosphine
TPPO	Triphenylphosphine Oxide

36

## 37 1. INTRODUCTION

38 One aviation concern is the jet fuel thermal stability. It is defined as the fuel's resistance to the  
39 formation of deposits under the influence of temperature that can lead to clogging and failure of  
40 the fuel injection system. These deposits are formed from soluble or insoluble precursors which  
41 can be formed at moderate temperatures between 140 and 250 °C through autoxidation  
42 phenomena. In this process, oxygen naturally dissolved in jet fuel (approximately 70 ppm) reacts  
43 with the hydrocarbon molecules by a free radical mechanism. The process is described in the  
44 literature as a three-step mechanism involving initiation, propagation (in two substeps) and  
45 termination [1]. It results in the formation of three classes of species: primary oxidation products  
46 (hydroperoxides [4]); secondary oxidation products (soluble oxidation products [5-10]) and  
47 Soluble Macromolecular Oxidation Reactive Species (SMORS) [11-14] or insoluble deposits  
48 [2,13-21].

49 It has been established that the thermal stability of jet fuel depends mainly on the operating  
50 conditions. These are the thermodynamic conditions (temperature [23-25], pressure [26-29]), time-  
51 dependent parameters (residence time [22], flow rate [29]), geometrical and technological  
52 characteristics (the nature of the materials [24,28,30-32] and the diameter [22,33,34] of the  
53 functional element under consideration), and the specific operating conditions (transient, steady  
54 state or shutdown phase) [35,36]. Beyond the conditions of use of jet fuel, several studies have  
55 shown that the deposit formation is mostly the result of the intrinsic physico-chemical properties  
56 of the fuel, such as its hydrocarbon composition and in particular the structure of the hydrocarbon

57 molecules, as well as interactions with oxygen [16,17,23,30,37,38] or trace species, such as  
58 heteroatomic species [39-49], dissolved metals [30,50-52] and additives [53,54]. These different  
59 factors do not necessarily act independently of each other, making autoxidation a very complex  
60 phenomenon.

61 Although the influence of these parameters has been reported in various studies, it is currently  
62 difficult to define the origin of the formation of precursor deposits. Several hypotheses were put  
63 forwards in the literature to explain their formation. However, no study has been able to determine  
64 the exact nature of the precursors and their formation mechanism. Recent investigations have  
65 highlighted the potential polar nature of these species, which may be derived from polymerization  
66 reactions [21] of soluble species or the precipitation of SMORS [14,20]. Other studies suggest an  
67 esterification reaction [15,16]. The formation of precursor deposits has also been proposed to be  
68 related to the difference in polarity between the carbonaceous molecules and the oxidized  
69 molecules formed, which would lead to demixing precipitation of the polar molecules formed [18].  
70 This phenomenon is more complex to understand when one considers the sulphur and nitrogen  
71 species in the jet fuel that may be involved in the deposit formation mechanism. Recent works  
72 have demonstrated the contribution of tools such as Density Functional Theory (DFT) calculations  
73 in proposing mechanisms for the reaction of hydroperoxides with polar molecules such as phenols  
74 and sulphur and nitrogen compounds to form SMORS or deposits [55-59].

75 To simplify the system and yet to better understand the autoxidation mechanisms of hydrocarbon  
76 species without sulphur and/or nitrogen species, it was proposed, in a previous work [10], to study  
77 the oxidation of n-dodecane, using the PetroOXY apparatus, for different advancements ( $\Delta P/P_{\max}$   
78 = 0 to 10 %) and temperatures (140-160 °C). Under these conditions, it was possible to identify  
79 and quantify the different products resulting from its degradation in the gas and liquid phases. In

80 addition, this study allowed the determination of the degradation mechanisms and the related  
 81 kinetic constants for linear alkanes. The aim of the present work is to complete the study started  
 82 with n-dodecane using the same methodology, in order to better understand the degradation  
 83 mechanisms specific to each molecular structural category of which jet fuel is composed. Five  
 84 model hydrocarbons were selected: n-dodecane and its isomeric mixture, n-butylcyclohexane,  
 85 1,2,4-trimethylbenzene and 1-methylnaphthalene). They were oxidized individually using the  
 86 PetroOXY apparatus, focusing on the onset of autoxidation ( $\Delta P/P_{\max} = 2-10\%$ ) at a temperature  
 87 and initial oxygen pressure of 160 °C and 700 kPa, respectively, to monitor the evolution of the  
 88 oxidation products as a function of reaction time. The same work was then carried out at  $\Delta P/P_{\max}$   
 89 = 10 %, an advancement sufficient to permit deposits, at three different temperatures (140, 150  
 90 and 160 °C) and an initial pressure of 700 kPa to determine the kinetic constants of degradation.

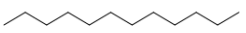
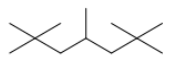
91 This methodology will allow to understand the behaviour of hydrocarbons under oxidative  
 92 conditions in the absence of sulphur and nitrogen containing molecules. This situation is likely to  
 93 become a reality as work is underway within the ASTM to approve the use of 100 % Synthetic  
 94 Alternative Fuels (SAF).

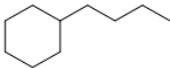
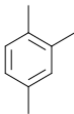
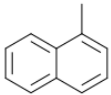
## 95 2. EXPERIMENTAL SECTION

### 96 2.1. Model molecules

97 Table 1 shows the characteristics of the 5 selected hydrocarbons.

*Table 1 - Properties of the selected hydrocarbon molecules*

Model compounds	Abbreviations	Molecular weight (g.mol <sup>-1</sup> )	Purity (%)	Structure
n-dodecane C <sub>12</sub> H <sub>26</sub>	n-C <sub>12</sub>	170.34	99	
n-dodecane isomers blend C <sub>12</sub> H <sub>26</sub>	n-C <sub>12</sub> IsoB	170.34	95	

<b>n-butylcyclohexane</b> <b>C<sub>10</sub>H<sub>20</sub></b>	n-BC	140.27	99	
<b>1,2,4-trimethylbenzene</b> <b>C<sub>9</sub>H<sub>12</sub></b>	1,2,4-TMB	120.19	98	
<b>1-methylnaphthalene</b> <b>C<sub>11</sub>H<sub>10</sub></b>	1-MN	142.20	96	

## 98 2.2. PetroOXY device

99 The PetroOXY device (Anton Paar) is used to measure the oxidation stability of fuels and oils.  
100 Measurements are compatible with ASTM D7525 [60], ASTM D7545 [61] (diesel, biodiesel and  
101 fatty acid methyl esters) and EN 16091 [62]. This device is widely used [63,64] and is one of the  
102 reference instruments for performing small scale rapid oxidation stability tests (RSSOT) on fuels.  
103 Among its advantages are the low sample volume needed, good repeatability and versatility, since  
104 it is possible to deviate from the standard conditions and vary a number of parameters (time,  
105 temperature, pressure).

106 5 mL of hydrocarbon were poured into a glass crucible. In order to assure that oxygen is the only  
107 dissolved gas, the fuel was degassed 2 min in an ultrasonic bath. The crucible was then introduced  
108 into a chamber hermetically closed. The tests were carried out at  $\Delta P/P_{\max} = 10\%$ , at an initial static  
109 oxygen pressure set at 700 kPa and at an initial temperature of 160 °C. Hydrocarbon degradation  
110 is indicated by the consumption of oxygen resulting in a drop in the pressure measured in the  
111 chamber. The induction period (IP) is defined as the time required for the pressure to be 10 %  
112 below the maximum test pressure. At the end of a test and after the apparatus was cooled, the gas  
113 phase was collected via the exhaust gas port into a dedicated cell, and the liquid and solid phases  
114 have been recovered after the cell was opened [65].

115 All the samples were tested 4 times to verify the repeatability and to have enough oxidized liquid  
116 to characterize.

117 The details of the calculations of the gasification rate and the conversion rates of reagents are  
118 described elsewhere [10].

## 119 **2.3. Characterization techniques**

### 120 2.3.1. Fourier Transform Infrared Spectroscopy

121 The gas, liquid and solid phases were analyzed by Fourier Transform Infrared Spectroscopy  
122 (FTIR) using a Frontier spectrometer (Perkin-Elmer). The analysis of the gas phase was carried  
123 out in transmission, recording 4 spectra in the 4000–1000  $\text{cm}^{-1}$  wavelength range, with a scanning  
124 speed of 0.2  $\text{cm}\cdot\text{s}^{-1}$  and a resolution of 4  $\text{cm}^{-1}$ . For the liquid and solid phases, a drop was deposited  
125 on a monoreflecting diamond and analyzed by Attenuated Total Reflectance (FTIR-ATR)  
126 equipped with a Mercury-Cadmium-Telluride detector. The same acquisition parameters were  
127 used as for the gas phase except that 5 spectra were recorded in the 4000–450  $\text{cm}^{-1}$  wavelength  
128 range.

### 129 2.3.2. Micro-Gas Chromatography

130 The gas phase was also analyzed by micro-Gas Chromatography ( $\mu$ -GC). The apparatus (Agilent  
131 4900) is equipped with Thermal Conductivity Detectors (TCD) and 3 columns:  $\text{Al}_2\text{O}_3$  (10 m  $\times$   
132 0.32 Internal Diameter (ID),  $T_{\text{column}} = 70\text{ }^\circ\text{C}$ ,  $P = 130\text{ kPa}$ ),  $\text{COx}$  (1 m  $\times$  0.7 ID,  $T_{\text{column}} = 80\text{ }^\circ\text{C}$ ,  $P$   
133 = 150 kPa), CP sil-5CB (20 m,  $T_{\text{column}} = 50\text{ }^\circ\text{C}$ ,  $P = 150\text{ ka}$ ). Helium and argon were vector gases.  
134 Calibration was performed before each test for  $\text{H}_2$ ,  $\text{CO}$ ,  $\text{CO}_2$ , and the hydrocarbon molecules.



### 135 2.3.3. Gas Chromatography-Mass Spectrometry

136 The liquid phase was analyzed by Gas Chromatography-Mass Spectrometry (GC-MS) with a  
137 Varian 450 GC/320 MS. This apparatus is equipped with a CP-8410 automatic sampler, a 1177  
138 split/splitless injector, a fused silica capillary column (phase type: VF-5 ms, length: 60 m, inner  
139 diameter: 0.25 mm, phase thickness: 1  $\mu\text{m}$ ) with a column flow of 0.8 mL/min and a Flame  
140 Ionization Detector (FID). The analysis was performed with helium as the vector gas. The injection  
141 temperature was set to 250 °C. The thermal program was optimized for all molecules: 5 min at 50  
142 °C; heating up to 175 °C (at a rate of 5 °C.min<sup>-1</sup>) for 5 min then to 250 °C (10 °C.min<sup>-1</sup>) for 45  
143 min. Standards were prepared by mixing various volumes of hydrocarbons and *n*-decane (purity  
144 > 99 %, Alfa Aesar) for alkanes and *n*-dodecane for aromatic model molecules. These standards  
145 and the oxidized samples were injected 3 times and a deviation of less than 1 % was imposed. The  
146 MS fragmentation was obtained by an electronic collision of 70 eV.

## 147 2.4. Quantification of the products formed

### 148 2.4.1. Identification of hydroperoxide species

149 The presence of hydroperoxide species has been demonstrated by the post reaction oxidation of  
150 triphenylphosphine (TPP) to the corresponding oxide Triphenylphosphine Oxide (TPPO)  
151 following the reaction [66,67]:



153 For this purpose, 4 g of TPP (99 %, Acros Organics) and 0.3 g of fluorene (>98 %, Acros Organics)  
154 were dissolved in 50 mL of chloroform ( $\geq$  99.8 %, Carl Roth). 250  $\mu\text{L}$  of this solution were added  
155 to 1 mL of oxidized model molecules and stirred for 10 min before analysis by GC and GC-MS.  
156 The detection limit of this method is less than 0.002 mM.

157 2.4.2. Peroxide Value

158 Peroxide species formed during the test were back-titrated using a method similar to that described  
159 in the standard ASTM D3703 [68], based on the reduction of the iodide molecules formed during  
160 titration with sodium thiosulphate. The Peroxide Value (PV) was calculated according to Equation  
161 1, where A and B are the volumes of a sodium thiosulphate solution of normality N added to a  
162 volume V of sample during the test and a blank test, respectively [67].

$$PV = \frac{((A - B) N \times 1000)}{V} \quad \text{Equation 1}$$

163 Four solutions were prepared for the determination of hydroperoxides:

164 (1) Revealing solution: 0.5 g of starch was dissolved in 50 ml of distilled water; the solution  
165 was brought to boil while stirring and then allowed to cool still stirring;

166 (2) NaI solution: 14.3 g of NaI (purity  $\geq 99\%$ , Sigma Aldrich) were dissolved in 10 mL of  
167 water under stirring;

168 (3) Dissolution solution: 30 mL of acetic acid (100 % purity, Carl Roth) and 20 mL of  
169 chloroform ( $\geq 99.8\%$  purity, Carl Roth) were mixed;

170 (4) Titrant solution: sodium thiosulphate (0.005 M)

171 The protocol consists of mixing, in an Erlenmeyer flask, 1 mL of the oxidized sample with 36.5  
172 mL of the dissolution solution. 500  $\mu\text{L}$  of the NaI solution were added while stirring. After 1  
173 minute, stirring was stopped and the conical flask was placed in a black box for 5 minutes. 37.5  
174 mL of iced water were then added as well as a few drops of the starch-revealing solution, used as  
175 a colour indicator, while stirring. The solution was titrated with the sodium thiosulphate solution  
176 using an automatic titrator with a precision of 2  $\mu\text{L}$ .

177 2.4.3. Total Acid Number

178 The Total Acid Number (TAN) is the mass of KOH required to neutralize the free acid molecules  
179 present in 1 g of sample [69]. The method used to determine the TAN is based on the standard  
180 ASTM D3242 [70]. It is an acid-basic titration, suitable in the range from 0.00 to 0.10 mg KOH/g.

181 Three solutions were prepared:

182 (1) iPOH/toluene solvent: 500 mL of toluene (purity  $\geq 99.8$  %, Carl Roth) and 495 mL of  
183 isopropanol (iPOH, purity  $\geq 99.5$  %, Carl Roth) were mixed and stirred manually before  
184 adding 5 mL of pure H<sub>2</sub>O;

185 (2) Titrant solution: 900 mL of iPOH were added to 100 mL of a solution of KOH in  
186 isopropanol (0.1 N, Carl Roth);

187 (3) Revealing solution: 0.1 g  $\pm$  0.01 g of solid phenolphthalein (J.T. Baker) were dissolved in  
188 50 mL H<sub>2</sub>O and 50 mL ethanol ( $\geq 90$  %, ALCOgroup).

189 The exact normality of the titrant solution was determined by colorimetric titration with a  
190 biphtalate solution of known concentration.

191 The acid number was determined as follows. 700  $\mu$ L of the oxidized sample were poured into a  
192 flask containing 40 mL of iPOH/toluene solvent and three drops of naphtholbenzeneine (CAS:  
193 145-50-6, Fisher Chemical) were added. This solution was titrated with the titrant solution under  
194 an inert nitrogen atmosphere using an automatic titrator with a precision of 0.02 mL.

195 2.4.4. Water Content

196 The water content was determined by coulometric titration using a Karl-Fisher titrator (Mettler  
197 Toledo C30 with a Pt electrode under 20  $\mu$ A). HYDRANAL Coulomat AK and HYDRANAL

198 Coulomat CGK solutions Honeywell Fluka) were used as anolyte and catolyte, respectively. The  
199 results were automatically collected and processed by the LabX software.  
200 For the analysis, 2 mL of oxidized sample were withdrawn with a syringe, weighted and placed  
201 into the Karl Fisher apparatus.

### 202 3. RESULTS

#### 203 3.1. Consumption of reagents

204 The selected molecules (Table 1) were oxidized using PetroOXY apparatus. As first, a temperature  
205 and an initial pressure of 160 °C and 700 kPa, respectively, were set. The reaction was stopped at  
206 low  $\Delta P/P_{\max}$  values (2, 4, 6, 8 and 10 %), in order to study the onset of the autoxidation process.  
207 Figure 1.a) shows the evolution of the pressure with reaction time for all the model molecules at  
208  $\Delta P/P_{\max} = 10\%$ . Except for 1-MN, for which the test durations are very long (3 to 10 h between  
209  $\Delta P/P_{\max} = 2$  and 10 %, respectively), the test durations for the other oxidized model molecules are  
210 short and vary from 20 to 40 min for 2 to 10 %. This suggests that diaromatic molecules have far  
211 the best oxidation stability among the selected model molecules. The IP deduced from these curves  
212 all follow a linear increase with  $\Delta P/P_{\max}$  in the range 2 to 10 %, as shown in Figure 1.b). This  
213 implies a constant rate of O<sub>2</sub> consumption within this  $\Delta P/P_{\max}$  range, regardless the nature of the  
214 molecule being oxidized.

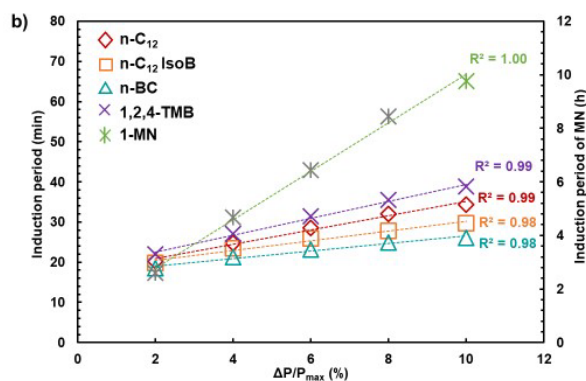
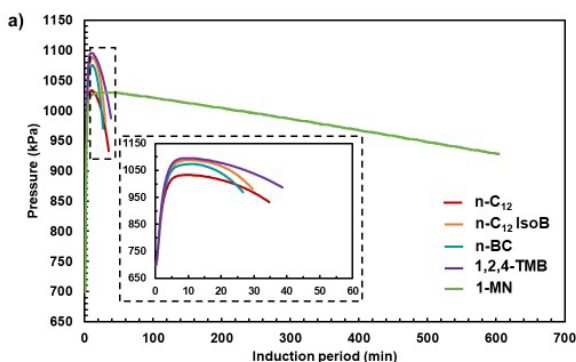


*Figure 1 - Oxidation evolution of model molecules at 160 °C and  $P_{O_2,i} = 700$  kPa with a) pressure versus duration time at  $\Delta P/P_{max} = 10$  % and b) induction period versus  $\Delta P/P_{max}$*

215  
216 The number of moles of O<sub>2</sub> and model hydrocarbon molecules consumed was monitored  
217 throughout the test (Figure S.M.1 in Supplementary Material). They both follow a linear trend as  
218 shown in Figure 2. O<sub>2</sub> consumption is higher for all the molecules and increases more rapidly than  
219 hydrocarbon consumption. In addition, the slopes, and therefore the consumption rates, are all  
220 different.

221 Assuming that one molecule of O<sub>2</sub> reacts with one molecule of hydrocarbon, the number of moles  
222 of reagents consumed would be expected to be equivalent. However, the O<sub>2</sub> consumption is much  
223 higher for all molecules except 1,2,4-TMB. At  $\Delta P/P_{max} = 10$  %, the O<sub>2</sub>/parent molecule molar  
224 ratios are 5:1, 7.8:1, 4.3:1 and 8.2:1 for the n-C<sub>12</sub>, n-C<sub>12</sub> IsoB, n-BC and 1-MN, respectively. This  
225 suggests that the oxygen reacts not only with the parent hydrocarbon but also with the oxidation  
226 products. In contrast, for the oxidation of 1,2,4-TMB, the O<sub>2</sub> consumption is close to that of the  
227 reagent with a molar ratio of 1.4:1.

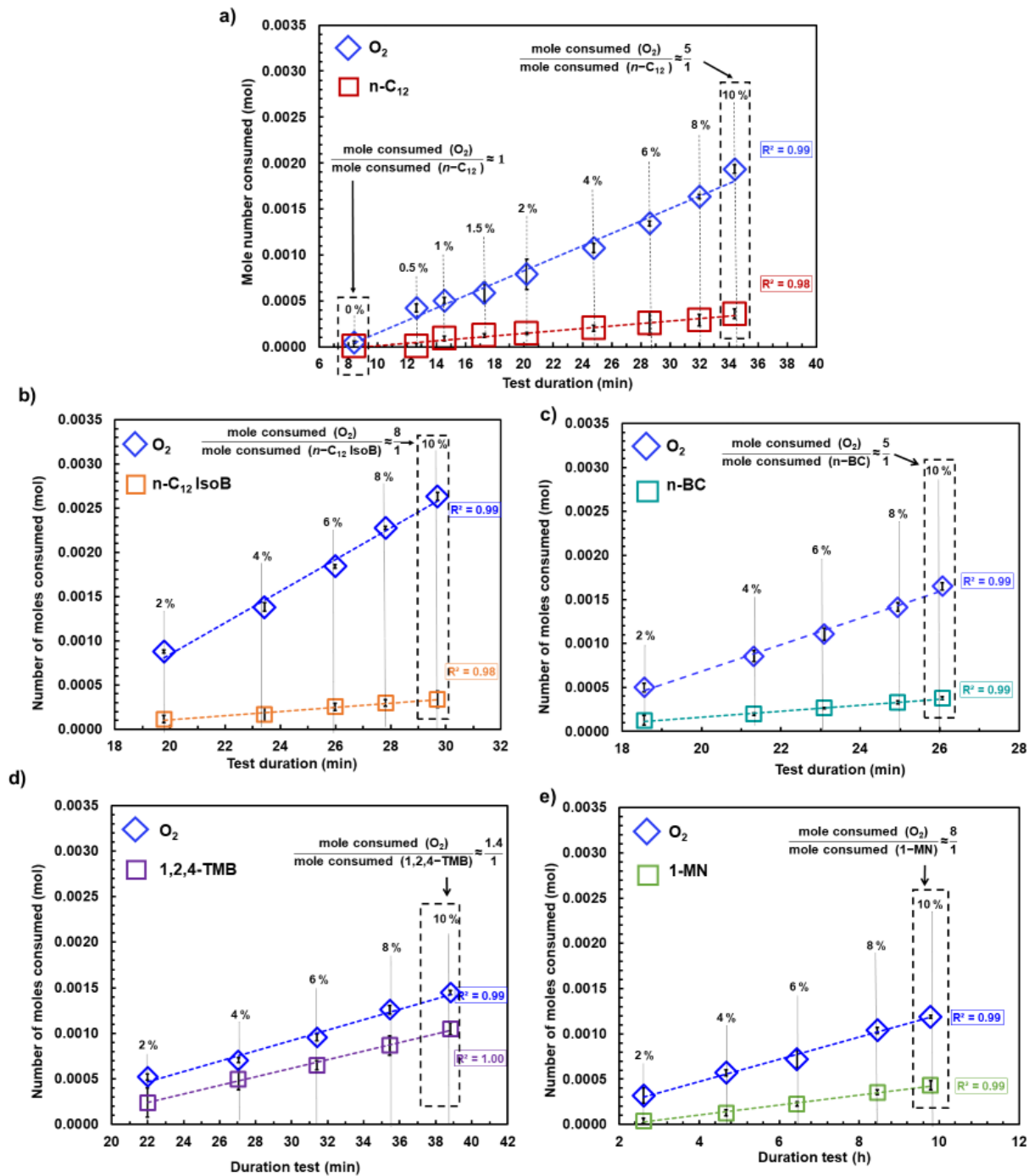


Figure 2 - Mole number of O<sub>2</sub> and model molecules consumed, with a) n-C<sub>12</sub>, b) n-C<sub>12</sub> IsoB, c) n-BC, d) 1,2,4-TMB and e) 1-MN, as a function of the duration test (T = 160 °C, PO<sub>2,i</sub> = 700 kPa, ΔP/P<sub>max</sub> = 10 %)

228 A second series of tests was conducted at three temperatures: 140, 150 and 160 °C at ΔP/P<sub>max</sub> = 10  
 229 % with an initial O<sub>2</sub> pressure of 700 kPa. The pressure evolution during the reaction shows similar  
 230 profiles. However, the maximum pressure reached increases with temperature while the time to

231 reach the target  $\Delta P/P_{max}$  decreases. (Figure S.M.2). Figure 3.a) shows the evolution of the  
 232 Induction Period as a function of temperature for the five hydrocarbons molecules. As expected,  
 233 the higher the temperature is, the shorter the IP is, confirming the influence of temperature as a  
 234 kinetic factor. Reagent consumption was also followed as a function of temperature increasing  
 235 with temperature (Figure 3.b). The  $O_2$  consumed is always higher than that of the model molecule,  
 236 but the ratio varies depending of the hydrocarbon oxidized.

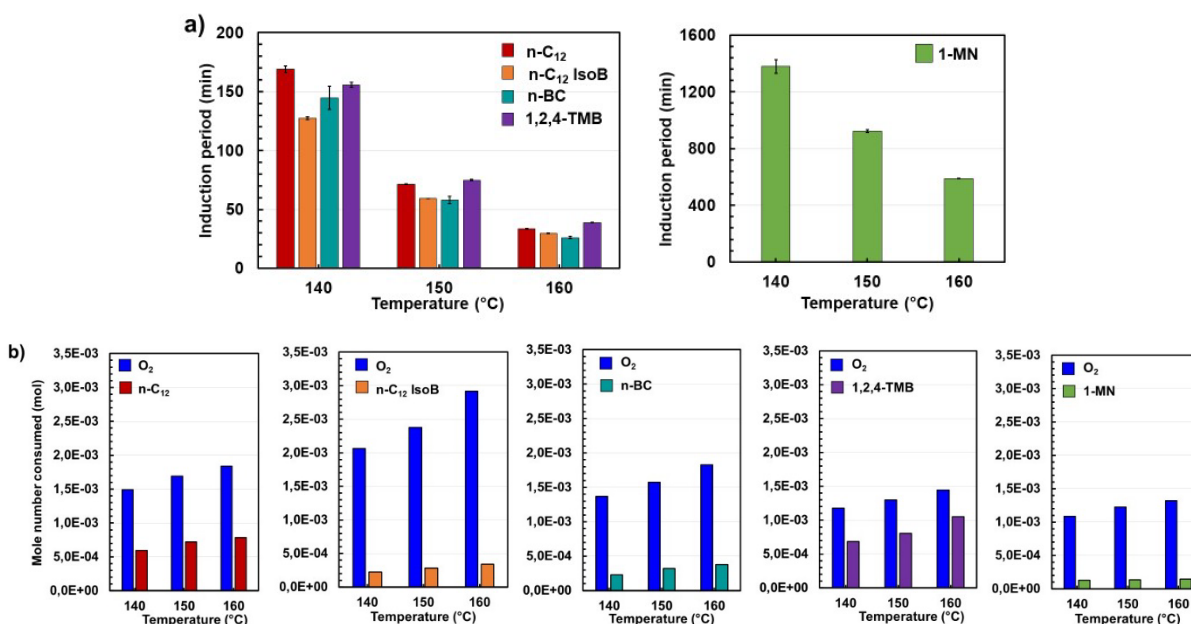


Figure 3 - Evolution as a function of temperature of a) the induction period and b) the mole number of  $O_2$  and model molecule consumed ( $\Delta P/P_{max} = 10\%$ ,  $P_{O_2,i} = 700$  kPa)

237

238  $O_2$  consumption rate depends on the chemical structure of the hydrocarbon studied, decreasing in  
 239 the following order: i-alkane  $\gg$  cyclo-alkane  $>$  n-alkane  $>$  mono-aromatic  $>$  di-aromatic.  
 240 For the model hydrocarbon molecules, their consumption rates follow the order: mono-aromatic  $>$   
 241 n-Alkanes  $>$  i-alkanes  $>$  cyclo-alkane  $>$  di-aromatic. This demonstrates the relationship between  
 242 the structure and the sensitivity of hydrocarbon differences to oxidation (Table S.M.3).

243

244 The quantitative analysis carried out in this study shows that the oxygen conversions at 140 and  
 245 160 °C are not identical for a fixed  $\Delta P/P_{\max}$ . Due to the temperature difference, the maximum  
 246 pressure ( $P_{\max}$ ) obtained in the batch system is not the same. This affects the calculation of  $\Delta P$  and  
 247 therefore the amount of oxygen consumed. To show the real effect of temperature, the tests should  
 248 have been performed at iso-conversion of oxygen, *i.e.* at the same oxygen consumption and not at  
 249 the same  $\Delta P/P_{\max}$ . Using the previously calculated oxygen consumption rates, it is easy to estimate  
 250 the additional time required. Note that this assumption was confirmed by performing tests with  
 251 corrected induction periods and iso-conversion of oxygen in the case of *n*-C<sub>12</sub>. [10] The corrected  
 252 IP are given in Table 2 and further used for the kinetic study.

Table 2 - IPs values obtained experimentally for different temperatures at  $\Delta P/P_{\max} = 10\%$  and after mathematical correction ( $P_{O_2,i} = 700$  kPa).

	<b>Temperature (°C)</b>	<b>140</b>	<b>150</b>	<b>160</b>
<b>1-MN</b>	Experimental IP (min)	1379	924	587
	<b>Corrected IP (min)</b>	<b>1676</b>	<b>993</b>	<b>587</b>
<b>1,2,4-TMB</b>	Experimental IP (min)	156	75	39
	<b>Corrected IP (min)</b>	<b>192</b>	<b>83</b>	<b>39</b>
<b>n-BC</b>	Experimental IP (min)	145	58	26
	<b>Corrected IP (min)</b>	<b>193</b>	<b>67</b>	<b>26</b>
<b>n-C<sub>12</sub></b>	Experimental IP (min)	169	71	33
	<b>Corrected IP (min)</b>	<b>209</b>	<b>78</b>	<b>33</b>
<b>n-C<sub>12</sub> IsoB</b>	Experimental IP (min)	127	59	30
	<b>Corrected IP (min)</b>	<b>180</b>	<b>73</b>	<b>30</b>

## 253 3.2. Analysis of the products formed

### 254 3.2.1 Gas phase

255 FTIR spectroscopy was first used to analyze the gas phase. Figure 4 shows the FTIR spectra of the  
 256 whole gas phase produced by the oxidation of the model molecules at  $\Delta P/P_{\max} = 10\%$  for  
 257 temperature and pressure fixed at 160 °C and 700 kPa, respectively.

258 Irrespective of the type of hydrocarbon, these spectra show:



- 259 • a band between 3500 and 3800  $\text{cm}^{-1}$  due to the stretching vibration  $\nu(\text{O-H})$  characteristic  
260 of alcohols and carboxylic acids;
- 261 • vibrational bands of the  $\text{CH}_2$  and  $\text{CH}_3$  groups,  $\nu(\text{C-H})$ , at 2850, 2935, 2970 as well as at  
262 1220, 1365 and 1455  $\text{cm}^{-1}$ , indicating the presence of carbon chains, which can be attributed  
263 both to the non oxidized molecules of interest and their oxidation products;
- 264 • a band at 2750  $\text{cm}^{-1}$  attributed to the  $\delta(\text{C-H})$  deformation vibration characteristic of  
265 aldehydes;
- 266 • a double band between 2300 and 2400  $\text{cm}^{-1}$  indicating the formation of carbon dioxide;
- 267 • a double band of the stretching vibration  $\nu(\text{C}\equiv\text{O})$  at 2120 and 2170  $\text{cm}^{-1}$  indicating the  
268 formation of carbon monoxide;
- 269 • a band at 1730  $\text{cm}^{-1}$  characteristic of the stretching vibration  $\nu(\text{C}=\text{O})$  due to ketone,  
270 carboxylic acid and aldehyde species.

271 Finally, a weak band at 3030  $\text{cm}^{-1}$ -and at 1680  $\text{cm}^{-1}$ , is observed, characteristic of the  $\nu(\text{C-H})$  and  
272  $\nu(\text{C}=\text{C})$  stretching vibrations of methane and alkenes, respectively.

273 The intensity of all these bands increases as the reaction progresses from  $\Delta P/P_{\text{max}} = 2$  to 10 %  
274 (Figure S.M.4.1.1.) and as the temperature increases from 140 to 160  $^{\circ}\text{C}$  (Figure S.M.4.1.2.). Note  
275 that the intensity of the bands at  $\Delta P/P_{\text{max}} = 10$  % is relatively similar for all model molecules except  
276 for n-C<sub>12</sub> IsoB for which it is tenfold greater. This indicates that the amount of products oxidized  
277 in the gas phase is largely promoted for branched alkanes.

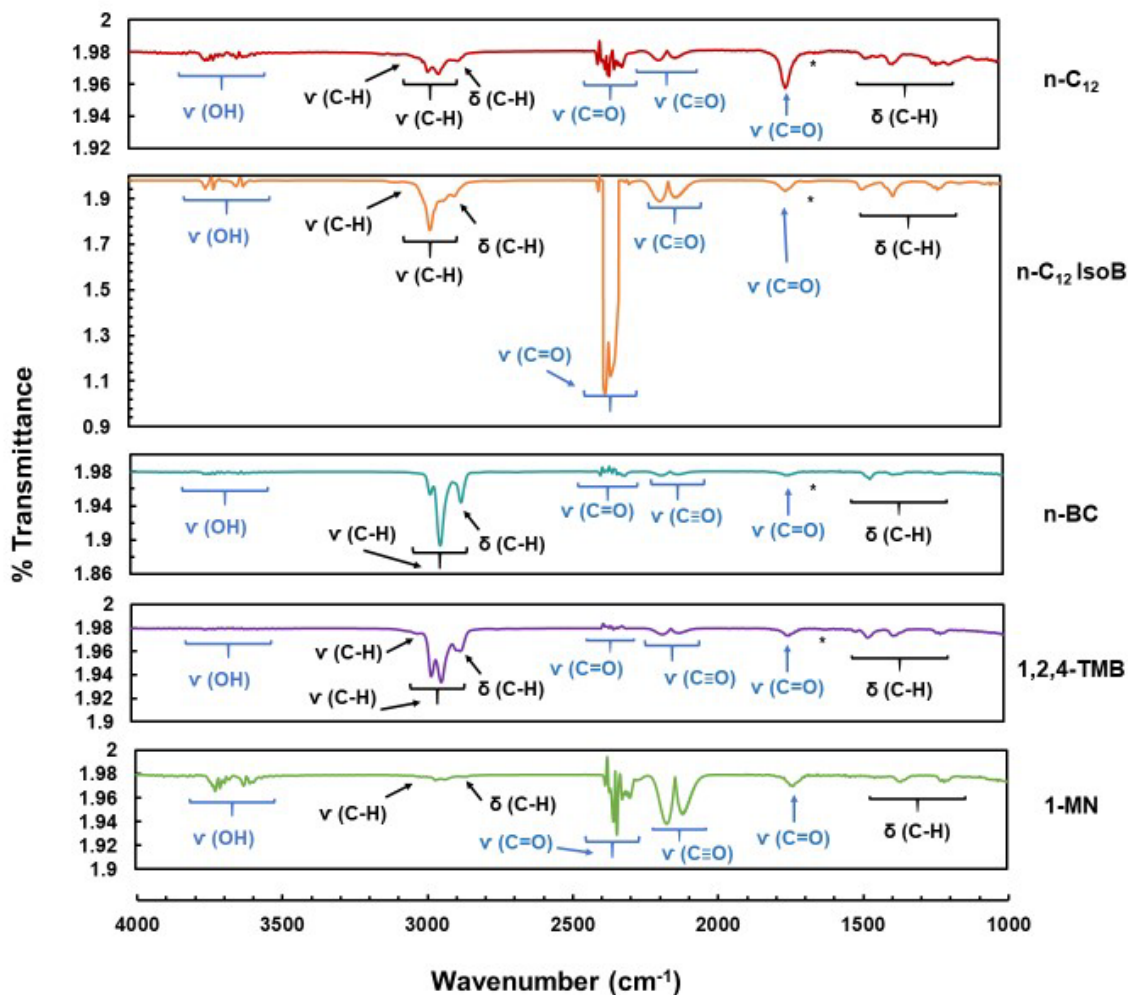


Figure 4 - FTIR spectra of the gas phase after model fuel oxidation; \* corresponds to the stretching vibration  $\nu_{(C=C)}$  characteristic of alkenes at  $1680\text{ cm}^{-1}$  ( $\Delta P/P_{\max} = 10\%$ ,  $T = 160\text{ }^{\circ}\text{C}$ ,  $P_{O_2,i} = 700\text{ kPa}$ )

278 The gas phase was further analyzed by  $\mu$ -GC for specific identification of the molecules formed.  
 279 The results indicate the formation of  $\text{H}_2$ ,  $\text{CO}_2$ ,  $\text{CO}$ ,  $\text{CH}_4$ ,  $\text{C}_2$ - $\text{C}_5$  alkanes and alkenes as well as polar  
 280 molecules such as water, formaldehyde, alcohols (methanol, ethanol, propanol) and acetone. This  
 281 is in line with the FTIR results. All these molecules start to form at an early stage,  $\Delta P/P_{\max} = 2$   
 282 % and their quantity increases as the reaction progresses (Figure S.M.4.2.1.). The chromatograms  
 283 obtained for experiments performed at different temperatures (Figure S.M.4.2.2.) show these same  
 284 molecules with an intensity that increases with temperature.

285 The volume of gaseous species detected on the CO<sub>x</sub> and Al<sub>2</sub>O<sub>3</sub> columns has been quantified.  
286 Overall, regardless of the parameter considered, a linear evolution of the gaseous products formed  
287 is observed (Figure S.M.4.2.3.). Figure 5 shows the volume percent gas results obtained at P/P<sub>max</sub>  
288 = 10 % and at fixed temperature and pressure of 160 °C and 700 kPa, converted to ppm  
289 concentration, CO<sub>2</sub>, H<sub>2</sub> and CO in Figure 5.a) and CH<sub>4</sub>, alkanes and alkenes in Figure 5.b). All the  
290 gases formed and identified are due to the formation of oxidation products in the liquid phase.  
291 Very little gas is formed (< 60,000 ppm *i.e.* 0.06 %) for all the oxidized model molecules. CO<sub>2</sub> is  
292 the main gas formed, whatever the oxidized molecule is (Figure 5.a). The other gases identified,  
293 in decreasing order, are: H<sub>2</sub>, CO, CH<sub>4</sub>, the alkenes and then alkanes; their gas volume never  
294 exceeds 0.01 %. (Figure S.M.4.2.3.)

295 CO<sub>2</sub> is produced in increasing amounts during oxidation of 1,2,4-TMB < n-BC < n-C<sub>12</sub> < 1-MN <  
296 n-C<sub>12</sub> IsoB (Figure 5.a). The branched alkane molecule gives off 40 times more CO<sub>2</sub> than the mono  
297 aromatic molecule. Moreover, the amount of CO<sub>2</sub> formed for 1-MN is at least twice that for n-C<sub>12</sub>  
298 and n-BC. This indicates a different oxidation reactivity depending of the molecule chemical  
299 structure. The influence of chemical structure is further confirmed by the results presented in  
300 Figure 5.b, showing that the amount of CH<sub>4</sub> produced by aromatic molecules (mono- and di-) is  
301 significantly higher than that produced by alkane molecules (linear, branched and cyclic). Thus,  
302 aromatic molecules tend to form more CH<sub>4</sub> while alkane molecules give gaseous alkenes.

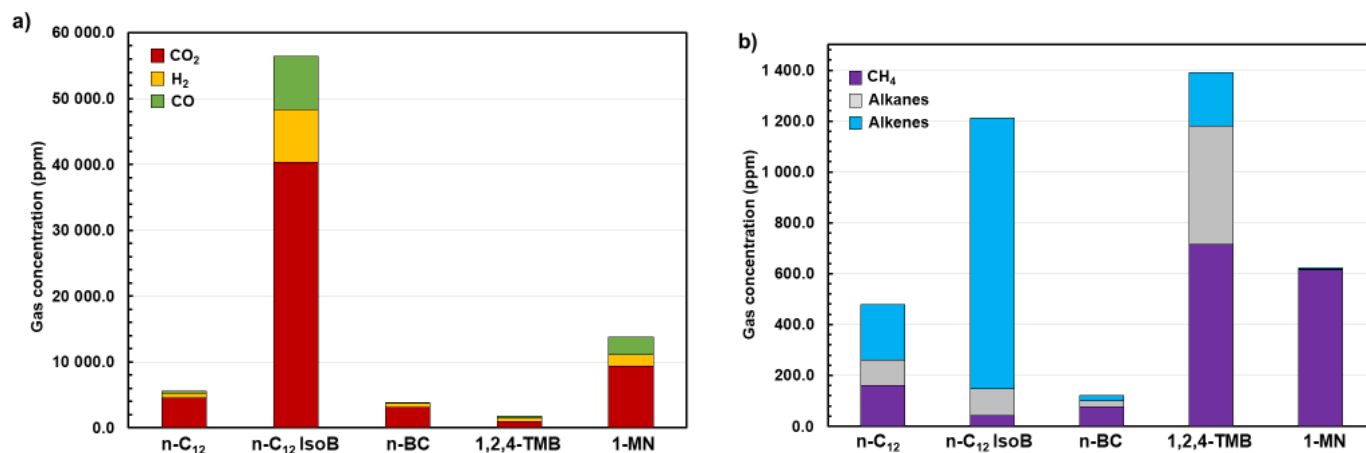


Figure 5 - Comparison of the amount of gas formed during the oxidation of the model molecules and determined from the quantitative analysis by  $\mu$ -GC ( $\Delta P/P_{max} = 10\%$ ,  $T = 160^\circ\text{C}$ ,  $P_{O_2,i} = 700\text{ kPa}$ )

### 303 3.2.2 Liquid phase

304 The liquid phase was analyzed by FTIR spectroscopy. The results obtained at  $\Delta P/P_{max} = 10\%$ , for  
 305 a temperature and pressure set at  $160^\circ\text{C}$  and  $700\text{ kPa}$  respectively, are shown in Figure S.M.5.1.

306 Except for the diaromatic molecule (1-MN), which shows no difference before and after oxidation,  
 307 the other spectra show a band between  $1710$  and  $1720\text{ cm}^{-1}$ , which can be attributed to the  $\nu(\text{C}=\text{O})$   
 308 stretching vibration characteristic of oxidized species of the ketone, aldehyde and/or carboxylic  
 309 acid type. In addition, in the case of 1,2,4-TMB, further bands are observed at  $3478$  and  $1334\text{ cm}^{-1}$   
 310 which can be attributed to  $\nu(\text{OH})$  and  $\delta(\text{OH})$  respectively, and two further bands at  $1212$  and  
 311  $1231\text{ cm}^{-1}$  corresponding to  $\nu(\text{C}-\text{O})$  stretching vibrations of alcohols and carboxylic acids.

312 To identify more precisely the oxidation products, the liquid phase was analyzed by GC-MS. The  
 313 products formed are identical and their quantity increases with test duration (Figures S.M.5.2.a. to  
 314 e.).

315 Figure 6.a.1. shows the peak of the unoxidized diaromatic molecule 1-MN with molecular mass  
 316  $M = 142\text{ g/mol}$  at  $40\text{ min}$  retention time and a series of peaks of variable molecular mass (from  
 317  $162$  to  $174\text{ g/mol}$ ), due to initial impurities (1-MN purity =  $96\%$ ). Most of the oxidation products

318 formed appear at retention times between 41 and 52 min (Figures S.M.5.3.a.1. and a.2.). These  
319 molecules include alcohols, aldehydes, and carboxylic acids. Two intense peaks are observed at  
320 45 and 47 min with molecular masses of 156 and 158 g/mol, respectively, which are attributed to  
321 1-naphthalaldehyde and 1-naphthalene methanol, respectively. Two further peaks with molecular  
322 masses of 172 g/mol, observed between 50 and 51 min, are assigned to 1 and 2-naphthalene  
323 carboxylic acids.

324 As for unoxidized 1,2,4-TMB, it is detected at a retention time of 27 min together with other lower  
325 peaks (molecular masses between 120 and 134 g/mol) corresponding to the initial impurities  
326 (Figures S.M.5.3.b.1. and b.2.). Five main oxidation products are formed (from 34 to 38 min.).  
327 Three are attributed to dimethyl-benzaldehyde molecules and two to phenyl methanol compounds  
328 (molecular masses 134 and 136 g/mol, respectively). A very low intensity peak attributed to  
329 dimethyl-benzoic acid ( $M = 150$  g/mol) was also observed as well as three intense peaks, between  
330 40 and 41 min, corresponding to products with molecular masses of 152 g/mol each, which could  
331 be hydroperoxides species.

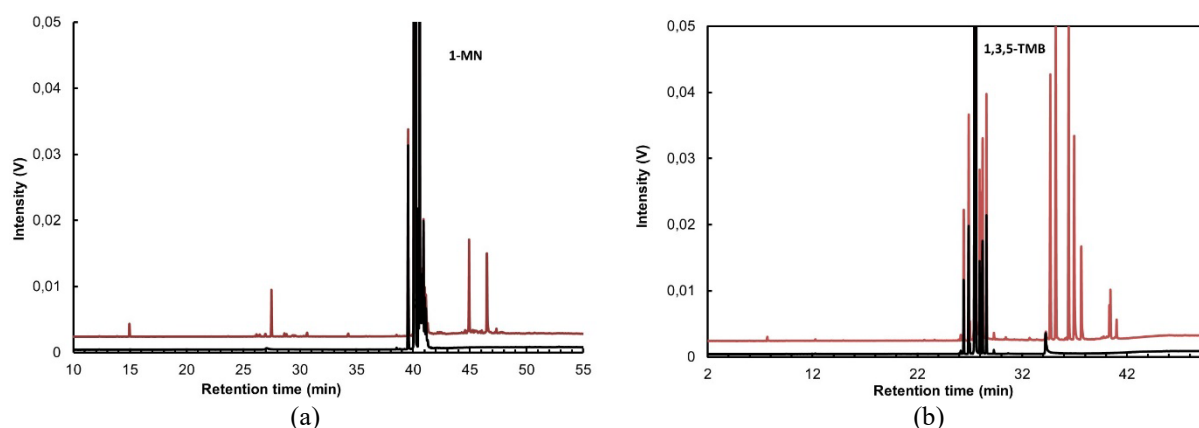


Figure 6 - Chromatograms obtained by GC-MS of the liquid phase before and after the oxidation of a) 1-MN and b) 1,2,4-TMB, with unoxidized molecules in black and oxidized molecules at  $\Delta P/P_{max} = 10\%$  in red ( $T = 160$  °C,  $P_{O_2,i} = 700$  kPa)

332 Several classes of compounds with different chain lengths are detected after the oxidation of alkane  
333 molecules (Figure 7). For n-BC oxidation, the molecules formed with a retention time of less than

334 28 min have a lower number of carbon atoms than the parent hydrocarbon (Figure S.M.5.4.a.1. to  
335 a.3.). The molecules identified are aldehydes, carboxylic acids, 2-ketones ( $m/z = 58$ ), secondary  
336 alcohols ( $m/z$  45 and 59). Primary and tertiary alcohols were also identified (fragments  $m/z$  31 and  
337 87, respectively) but in smaller amounts. Molecules detected between 34 and 38 min were mostly  
338 alcohols and ketones with the same carbon number as n-BC: X-butyl-cyclohexanol and X-butyl-  
339 cyclohexanone. No X-butyl-cyclohexanal or X-butyl-cyclohexanoic acid was detected. This does  
340 not mean that they were not formed: the boiling temperature of these species is very high (230 and  
341 288 °C, respectively) and they may not evaporate during the GC injection. Finally, about ten peaks  
342 between 40 and 45 min show the  $m/z$  139 fragment. These peaks are attributed to X-butyl-  
343 cyclohexane hydroperoxides.

344 The oxidation of n-C<sub>12</sub> gives molecules with a retention time below 34 min, corresponding to  
345 shorter carbon chains than the parent hydrocarbon (Figure 7.b). As for n-BC, for a fixed chain  
346 length, three types of compounds were identified: a ketone, an aldehyde and a carboxylic acid  
347 (Figures S.M.5.4.b.1. to b.3.). Most of the ketones identified show the  $m/z$  58 fragment  
348 characteristic of 2-ketones. Alcohols are also observed and most of them have the  $m/z$  45 and 59  
349 fragments which are characteristic of secondary alcohols. Smaller amounts of primary alcohols  
350 ( $m/z$  31) and dodecanal were also identified. The molecules detected at retention times between  
351 42 and 46 min have the same chain length as n-C<sub>12</sub>. These are alcohols and ketones, X-dodecanol  
352 and X-dodecanone with positions X = 1 to 6 [10,71]. Finally, peaks close to 53 min with  $m/z$  169  
353 characteristic of hydroperoxide species  $[M - \bullet\text{OOH}]^+$  [72] were detected. In a previous study it was  
354 confirmed that these were dodecyl hydroperoxide isomers [10].

355 For the branched alkane C<sub>12</sub> IsoB, the compounds detected at retention times below 27 min have  
356 shorter chain lengths (C<sub>1</sub> to C<sub>8</sub>) than the model molecule (Figure 7.c). As for the linear alkanes,

357 the compounds identified for these low retention times are 2-ketones ( $m/z$  58), secondary alcohols  
358 in the majority ( $m/z$  45), some tertiary alcohols ( $m/z$  59 and 87) and carboxylic acids in very small  
359 quantities. No aldehyde-type molecules were detected. The peaks between 22 and 33 min  
360 correspond to the approximately forty isomers constituting n-C<sub>12</sub> IsoB mixture (Figure  
361 S.M.4.4.c.1. to c.2.). In this same retention time range, many fragments previously absent for the  
362 non-oxidized n-C<sub>12</sub> IsoB are observed, thus characterizing the oxidized products formed. These  
363 include products such as primary ( $m/z$  31) and secondary alcohols ( $m/z$  45, 59 and 73), ketones  
364 ( $m/z$  43 and 58), aldehydes ( $m/z$  44, 75 and 31) and carboxylic acids ( $m/z$  60). This suggests that  
365 alcohol, aldehyde, and carboxylic acid molecules are present but co-eluted. Most species with  
366 retention times above 40 min are primary alcohols ( $m/z$  31) and hydroperoxide species [M -  
367 •OOH]<sup>+</sup> ( $m/z$  169).

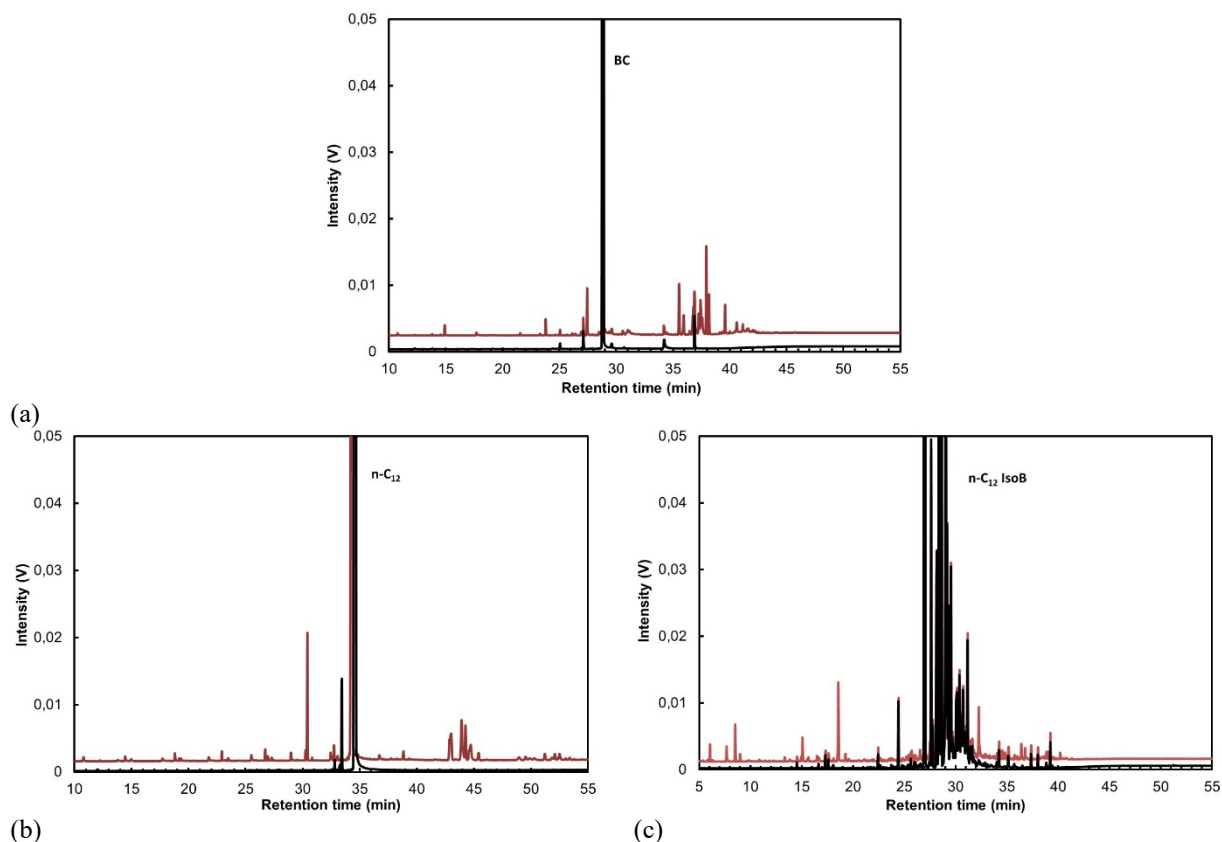


*Figure 7 - Chromatograms obtained by GC-MS, of the liquid phase before and after the oxidation of a) n-BC, b) n-C<sub>12</sub> and c) C<sub>12</sub> IsoB, with unoxidized molecules in black and oxidized molecules at  $\Delta P/P_{max} = 10\%$  in red ( $T = 160\text{ }^{\circ}\text{C}$ ,  $P_{O_2,i} = 700\text{ kPa}$ )*

368 Consequently, as for n-C<sub>12</sub> experimental study [10], GC-MS analysis revealed the presence of  
369 fragments with m/z ratios attributable to hydroperoxide species  $[M - \bullet\text{OOH}]^+$  [72]. In the case of  
370 the aromatic molecules, there is one for 1-MN and three for 1,2,4-TMB. In the case of alkane  
371 molecules, there are 8 for n-BC and 6 for n-C<sub>12</sub>. To confirm their presence, an indirect assay based  
372 on their reduction to alcohols with TriPhenylPhosphine (TPP) was carried out. The intensity of the  
373 alcohols should increase as the TPP is oxidized to TriPhenylPhosphine Oxide (TPPO) if the peaks  
374 present in Figure 6 and Figure 7 correspond to hydroperoxides. This is exactly what is observed,  
375 confirming the peaks assignments to hydroperoxides of the oxidized model molecules (Figure  
376 S.M.5.5.).

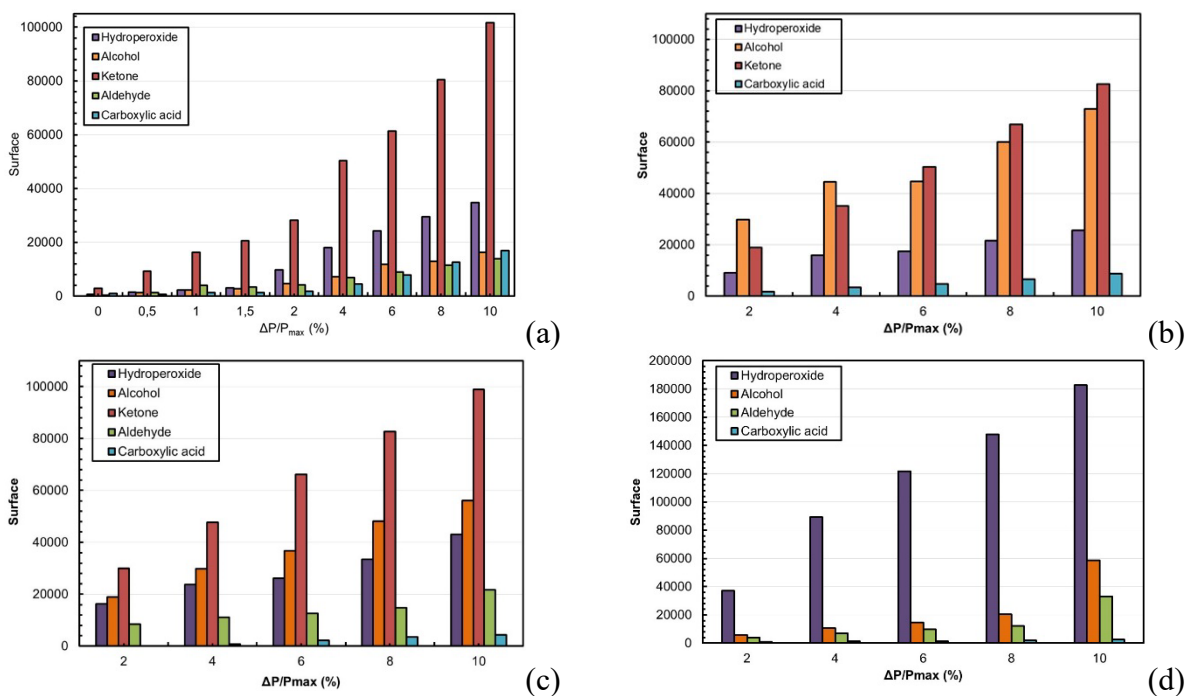
377 For aromatic molecules there is one peak for 1-MN and three peaks for 1,2,4-TMB. Given the  
378 initial chemical molecule structures, it is possible to correlate the number of peaks attributed to  
379 hydroperoxides with the number of branched methyl groups in the molecules.

380 For alkane molecules, the same correlation can be made between the number of peaks assigned to  
381 hydroperoxide isomers and the molecule chemical structures. In the case of n-BC, 8 peaks are  
382 observed, indicating the presence of 8 X-butyl cyclohexane hydroperoxides and for n-C<sub>12</sub>, 6 peaks  
383 associated with 6 X-dodecyl-hydroperoxides are observed.

384 For the branched alkane molecule (C<sub>12</sub> IsoB), the complexity of the isomeric mixture meant that it  
385 was not possible to assign all the hydroperoxides formed. However, GC-MS analysis revealed the  
386 presence of several fragments characteristic of primary alcohols (m/z 31) (Figure 7.c.). The  
387 oxidation of hydroperoxides by TPP exacerbated peaks present in this region (Figure S.M. 5.6)  
388 which can therefore be attributed to alcohols. All these elements support the presence of several  
389 hydroperoxides, which could not be detected due to a co-elution phenomenon.



390 To perform a quantitative GC analysis it is necessary to use standards. There are too many products  
 391 formed in the liquid phase to be able to calibrate all of them. A semi-quantitative analysis was  
 392 therefore carried out by comparing peak surface areas. The cumulative surface area of each family  
 393 of compounds was measured and plotted for increasing  $\Delta P/P_{\max}$  (Figure 8). The amount of primary  
 394 (hydroperoxides) and secondary (alcohols, ketones, carboxylic acids...) oxidation products  
 395 formed varies depending on the nature and structure of the hydrocarbon molecule oxidized. For  
 396 alkane molecules, Figure 8.a. to c. shows that the products are formed in the following proportions:  
 397 ketone > alcohol and hydroperoxides > aldehydes and carboxylic acids. For 1,2,4-TMB,  
 398 hydroperoxides are formed in majority while it is the opposite for 1-MN. The trend is reversed for  
 399 the alcohols and aldehydes formed. Moreover, whatever the aromatic molecule structure is, the  
 400 amount of acid molecules formed is very small.



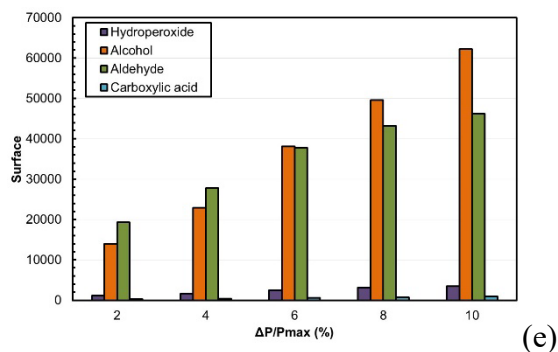


Figure 8 - Evolution of the oxidation products formed in the liquid phase obtained by GC of a) n-C12 [10], b) n-C12 Iso B, c) n-BC, d) 1,2,4-TMB and 1-MN at different advancements ( $T = 160$  °C,  $PO_{2,i} = 700$  kPa)

401

402 Peroxide Value (PV), Total Acid Number (TAN) and water content titrations were performed to

403 confirm the semi-quantitative GC results (Figure 9).

404 The PV increases linearly and significantly for the model molecules between  $\Delta P/P_{max} = 2$  and

405 10%, except for n-BC and n-C12 IsoB for which it follows a logarithmic trend (Figure 9. a.). Note

406 that the PV varies depending on the nature of the model molecule oxidized and the amount of

407 hydroperoxide formed follows this order: 1-MN < n-C<sub>12</sub> IsoB < n-C<sub>12</sub> ~ n-BC < 1,2,4-TMB.

408 The TAN results (Figure 9.b) confirm an increasing amount of acid species as the reaction

409 progresses. Furthermore, n-C<sub>12</sub> IsoB gives the highest quantity of carboxylic acids (~ 6 mg KOH/g

410 at  $\Delta P/P_{max} = 10$  %), while the other molecules form almost twice as few acids (TAN < 2.5 mg

411 KOH/g). The TAN values evolve following the order: 1,2,4-TMB < 1-MN < n-BC < n-C<sub>12</sub> << n-

412 C<sub>12</sub> IsoB.

413 The amount of water produced increases significantly for all oxidized molecules. The molecule

414 that forms the largest amount of water is the 1,2,4 -TMB (508 to 1780 ppm between  $\Delta P/P_{max} = 2$

415 and 10 %). For the other molecules, the water content is always less than 500 ppm and the amount

416 formed varies in the following order: n-C<sub>12</sub> IsoB < n-BC < 1-MN < n-C<sub>12</sub> << 1,2,4-TMB.

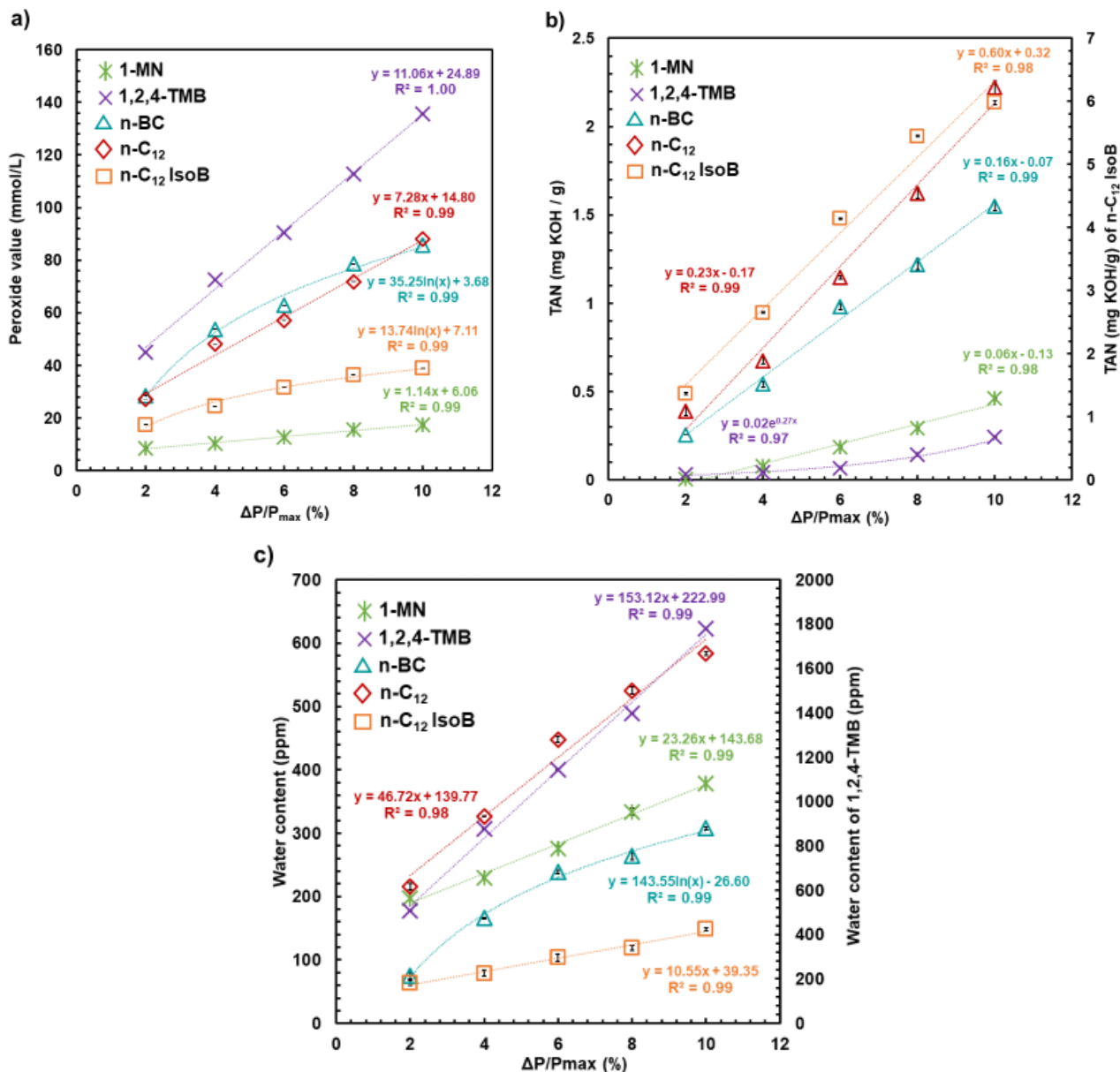


Figure 9 – Evolution of a) Peroxide Value (PV), b) Total Acid Number (TAN) and c) water content, formed in the liquid phase by oxidation of the model molecules at different  $\Delta P/P_{max}$  ( $T = 160$  °C,  $P_{O_2,i} = 700$  kPa)

417

418 Overall, the hydroperoxide, acid and water contents are related. This was particularly observed for

419 alkane molecules (linear, branched and cyclic): when the hydroperoxide concentration is high, the

420 acid content is low but the water content is high. In addition, the acid content depends on the

421 number of primary carbon atoms in the molecule. The aromatic molecules have different patterns

422 of hydroperoxide formation and consumption depending on the number of rings they have, which

423 has a direct impact on the amount of secondary products. Typically, the di-aromatic molecule  
424 showed a lower amount of primary oxidation products compared to the mono-aromatic molecule,  
425 indicating a higher hydroperoxide consumption rate. This rapid conversion of primary oxidation  
426 products should involve a significant amount of secondary oxidation products, namely aldehydes,  
427 carboxylic acids and water molecules. This is highlighted by the higher TAN measured. However,  
428 the water content does not follow this reasoning. Indeed, for the di-aromatic molecule, the water  
429 content is 5 times lower than for the mono-aromatic molecule.

430 Based on the previous observations, water molecules could be formed by:

- 431 • the decomposition of hydroperoxides;
- 432 • the oxidation of aldehydes to carboxylic acids;
- 433 • the reaction of elimination of hydrogen from a methyl group substituting the aromatic rings.

### 434 3.2.3 Solid phase

435 Except for n-C12, a residual gel was observed at the bottom of the vial after the oxidation tests  
436 (Figure 10). The aspect of the deposit varies according to the initial nature of molecule: droplets  
437 for the alkane molecules (n-C<sub>12</sub> IsoB and n-BC) and a thin layer for the aromatics molecules (1,2,4-  
438 TMB and 1-MN).

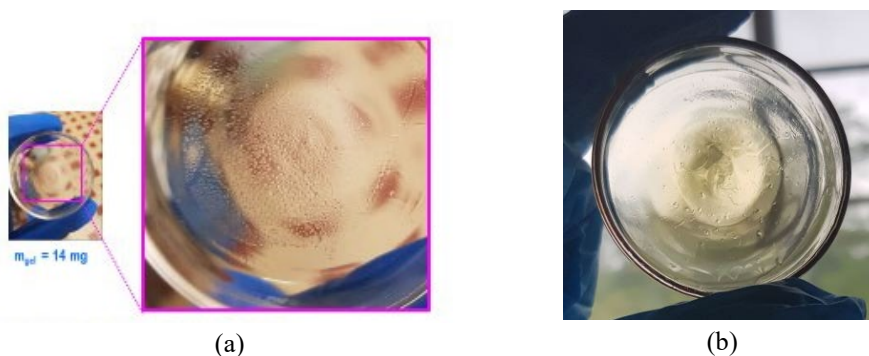


Figure 10 – Gel formed after n-C<sub>12</sub> IsoB (a) and MN-1 (b) oxidations ( $T = 160$   
 $^{\circ}\text{C}$ ,  $P_{\text{O}_2} = 700 \text{ kPa}$ ,  $\Delta P/P_{\text{max}} = 10 \%$ )

439 Due to the small quantity available, it was only possible to characterize the gels by FTIR after  
440 dissolution in acetonitrile (ACN). By comparing the spectra of each oxidized molecule with those  
441 of the gel dissolved in ACN, the appearance of additional bands was observed (Figure S.M.6.).

442 In the case of alkane molecules (n-C<sub>12</sub> IsoB and n-BC), the results showed three additional bands:

- 443 • at 1150 cm<sup>-1</sup> attributed to the stretching vibration  $\nu_{(C-O)}$  characteristic of carboxylic acids;
- 444 • at 1640 cm<sup>-1</sup> attributed to the stretching vibration  $\nu_{(C=C)}$ ;
- 445 • a large band between 3200 and 3700 cm<sup>-1</sup> attributed to the stretching vibration  $\nu_{(O-H)}$   
446 characteristic of alcohols and carboxylic acid functions.

447 These results indicate that the gels formed for n-C<sub>12</sub> IsoB and n-BC are composed of significant  
448 amounts of acidic species (Figure S.M.6.1). This may explain why a low TAN value was measured  
449 in the liquid phase. It can be assumed that this gel is composed of acid molecules that have  
450 precipitated at the bottom of the crucible due to the polarity difference [18]. It is also clear that  
451 oxidized products such as ketones and carboxylic acids can be further oxidized. This is even more  
452 likely if the carbon chain of the selected alkane molecules is long and this could lead to esters,  
453 lactones, furanones, etc. This gel could be a precursor of the deposit.

454 In the case of 1,2,4-TMB and 1-MN, a thin gel layer was observed and this gel was in higher  
455 amounts than for alkanes (Figures S.M.6.2 and S.M.6.3). The presence of polar species of carbonyl  
456 type such as possibly carboxylic acids or hydroperoxides was also highlighted. Indeed, bands  
457 characteristic of the stretching vibrations  $\nu_{(O-H)}$ ,  $\nu_{(C=O)}$  and  $\nu_{(C-O)}$  at 3476, 1738 and 1213 cm<sup>-1</sup>, were  
458 observed. and an intense band around 800 cm<sup>-1</sup>, which can be associated to a polymerization  
459 reaction based on the literature results [79-82], was detected. Although it was difficult to precisely  
460 assign this band to a functional group, several literature references suggest that it could be:

- 461 • an off-plane deformation band of the aromatic C-H bonds (between 750 and 870  $\text{cm}^{-1}$  for  
462 mono-substituted C-H, 815  $\text{cm}^{-1}$  for di-substituted C-H and 750  $\text{cm}^{-1}$  for a quadruple  
463 substitution). This is the most likely explanation because stretching vibrations  $\nu_{\text{(C-H)}}$  are  
464 observed around 3030  $\text{cm}^{-1}$ . This assignment would suggest that the gel obtained would be  
465 mainly composed of aromatic molecules with a carboxylic acid function. Furthermore, the  
466 quantitative results showed that the acid species are present in very small quantities in the  
467 liquid phase. It can therefore be assumed that the benzoic acids formed in the liquid phase  
468 precipitated at the bottom of the vial to form a gel;
- 469 • a characteristic band of the C-O-C bond. Many literature references [79,80,85,86] indicate  
470 that this bond, combined with the stretching vibration  $\nu_{\text{(O-H)}}$  at 3476  $\text{cm}^{-1}$ , is visible during  
471 a polymerization reaction and could explain the gel texture [81]. The polymerization  
472 mechanisms are shown in Figure S.M.6.4.1. ;
- 473 • a stretching vibration  $\nu_{\text{(O-O)}}$  characteristic of the peroxy group, which can be attributed to  
474 hydroperoxide type molecules [82,87]. This would imply that the gel formed for 1-MN  
475 results from hydroperoxide molecules precipitation formed in the liquid phase. This is not  
476 probable for 1,2,4-TMB because the liquid quantitative analysis showed a significant  
477 amount of hydroperoxides. However, it is possible to envisage a polymerization reaction  
478 between an alkyl peroxide radical and an alkyl radical  $\text{R}\cdot$  or between two carboxylic acid  
479 molecules linked together by an O-O bond (Figure S.M.6.4.2.).

480 All these elements suggest that the recovered gel contains polar compounds (especially carbonyl  
481 functions) in significant quantities. Consequently, the precipitation of polar molecules can be  
482 assumed, which could generate a polymerization reaction in the gel [18]. This result also shows

483 that the formation of SMORS or insoluble deposits do not require the presence of molecules  
484 containing sulphur or nitrogen atoms.

## 485 **4. DISCUSSION**

### 486 **4.1. Highlighting chemical structure influence on autoxidation mechanism reactivity**

487 In the liquid phase, the oxidation products formed are identical within a class of oxidized model  
488 molecules and their quantity increases as the reaction progresses. This implies that for any degree  
489 of advancement within the range considered ( $\Delta P/P_{\max} = 2$  to 10 %), the mechanisms involved are  
490 also identical.

491 For all oxidized model molecules, hydroperoxides species are always formed. The secondary  
492 oxidation products vary according to the structure of the initial molecule, *i.e.* depending whether  
493 it is linear, branched, cyclic or aromatic. In the case of alkane molecules, the oxidized products  
494 formed are primary and secondary alcohols, ketones, aldehydes, and carboxylic acids. The same  
495 applies to aromatic molecules but without the secondary alcohols and ketones. Based on these  
496 findings, it is possible to divide the products formed into different classes according to the initial  
497 structure of the model molecules. In the case of aromatic molecules, we distinguish them into two  
498 classes: hydroperoxides and oxidized products with a carbon chain equal to that of the initial  
499 molecule. In the case of alkane molecules, a third class of oxidation products is observed: products  
500 with a shorter carbon chain.

#### 501 **4.1.1 The hydroperoxides**

502 Hydroperoxides result from the propagation step, which is divided into two sub-steps. The first  
503 sub-step involves the reaction between an alkyl radical  $R\bullet$  and an  $O_2$  molecule to form a peroxide  
504 radical  $RO_2\bullet$ , followed by a second sub-step, in which the latter can remove a hydrogen atom from  
505 a hydrocarbon molecule  $RH$  present in the environment to form hydroperoxide species ( $ROOH$ ).

506 Based on the experimental results, it has been established that, for a given hydrocarbon molecule,  
507 the available H atoms induce a number of possibilities for O<sub>2</sub> attacks to form a peroxide radical.  
508 This has been demonstrated in particular in the case of the oxidation of aromatic molecules, where  
509 TPP results have shown a direct correlation between the number of methyl groups present in the  
510 initial molecule and the hydroperoxides formed. Similarly, for alkane molecules, the number of H  
511 atoms in the carbon chain can also be used to predict the number of hydroperoxides formed,  
512 provided that the symmetry elements attributed to the chemical structure of these molecules are  
513 taken into account.

#### 514 *4.1.2. Oxidized products with carbon chain length equal to the initial hydrocarbon molecule*

515 The hydroperoxides formed will decompose into alkoxy radicals RO• and hydroxyl radicals OH•.  
516 These species will then react with the other molecules to form alcohols and water, according to  
517 Reaction 1 and Reaction 2.



518 This mechanism is consistent with the results obtained as it can explain the decomposition of  
519 hydroperoxides into alcohols as well as the formation of water. Depending on the nature of the  
520 carbon attacked, the ROOH species formed will lead to the formation of a primary, secondary or  
521 tertiary alcohol. If a primary alcohol is formed (hydrogen attack at the end of the chain), oxidation  
522 continues, leading to the formation of an aldehyde and then a carboxylic acid. If a secondary  
523 alcohol is formed, it oxidizes to a ketone.-The mechanisms of formation of these oxidation products  
524 have been described in detail in a previous paper [10]. In addition, the oxidation products formed  
525 will have a chain length with a number of carbon atoms equal to the chain length of the initial  
526 model molecule.



527 For alkane molecules, namely for n-BC and n-C<sub>12</sub>, the oxidation products are a mixture of primary  
 528 and secondary alcohols, ketones, aldehydes, and carboxylic acids. The amount of secondary  
 529 alcohols is higher than that of primary alcohols as shown in *Table 3*. It is interesting to note that the  
 530 area ratio of the primary to secondary alcohols does not vary much with the reaction temperature.  
 531 For n-C<sub>12</sub>, if the probabilities of formation of each alkyl radicals from n-dodecane are equivalent,  
 532 1/6 of the total alcohols produced should be primary and 5/6 secondary alcohols. Thus, the  
 533 expected area ratio of primary to secondary alcohols should be 0.20; the experimental values  
 534 obtained are very close, between 0.16 and 0.18. For n-BC, 1/10, 8/10 and 1/10 of the alcohols  
 535 should be primary, secondary and tertiary alcohols respectively, if an equivalent probability of  
 536 formation of alkyl radicals was observed. Thus, the theoretical ratio of the surface areas of the  
 537 primary/secondary alcohols expected should be 0.125 and that of the tertiary/other alcohols 0.135.  
 538 Again, the experimental values obtained are very close, *i.e.* 0.12 to 0.14 for the first ratio and 0.11  
 539 to 0.13 for the second one (*Table 3*).

540 In the case of the branched alkane molecule (n-C<sub>12</sub> IsoB), it was difficult to determine the nature  
 541 of the molecules formed by GC-MS due to a co-elution phenomenon.

*Table 3 - Surface areas ratios obtained by GC for alcohols formed in the liquid phase for all model molecules ( $\Delta P/P_{max} = 10\%$ ,  $P_{O_2,i} = 700\text{ kPa}$ ).*

Temperature (°C)	140	150	160
$n\text{-C}_{12}$ area ratio = $\frac{\text{surface of primary alcohol}}{\Sigma \text{surfaces of secondary alcohols}}$	0.16	0.17	0.18
$\text{C}_{12}$ IsoB area ratio = $\frac{\text{surface of primary alcohol}}{\Sigma \text{surfaces of secondary alcohols}}$	0.18	0.20	0.22
BC area ratio = $\frac{\text{surface of primary alcohol}}{\Sigma \text{surfaces of secondary alcohols}}$	0.12	0.12	0.14
BC area ratio = $\frac{\text{surface of tertiary alcohol}}{\Sigma \text{surfaces of primary and secondary alcohols}}$	0.11	0.12	0.13

542

543 The oxidation products of 1,2,4-TMB obtained in the liquid phase are of the following types:  
544 benzene hydroperoxides, benzoic alcohols, benzaldehydes and benzoic acids. The structure of  
545 TMB explains this result as only the hydrogen atoms of the 3 methyl groups can react with  
546 dioxygen. This leads to the formation of three hydroperoxides, all of which are formed on primary  
547 carbons, producing three primary alcohols, three aldehydes and three carboxylic acids. In addition,  
548 the benzene ring is not opened and therefore does not undergo a chain breaking reaction. Therefore,  
549 no products are formed with a lower number of carbon atoms than TMB, only molecules of the  
550 same size (*i.e.* 9 carbon atoms).

551 For 1-MN, most of the products are derived from the oxidation of the molecule at a preferential  
552 position: one of the hydrogen atoms of the methyl group. The resulting products are therefore: 1-  
553 methyl naphthalene hydroperoxide, a primary alcohol, 1-naphthalene methanol, an aldehyde, 1-  
554 naphthalaldehyde and a carboxylic acid, 1-naphthalene carboxylic acid. In total, the oxidation  
555 products have the same size as the molecule of interest, *i.e.* 11 carbon atoms. Once again, the  
556 aromatic structure of the molecule, and in particular the two benzene rings, is very stable and does  
557 not allow for a chain breaking mechanism, which explains the reduced number of molecules  
558 formed, under the conditions of the tests. On this basis, and given the nature of the branching of  
559 the aromatic molecules tested, it is not surprising that no ketone-type products were identified,  
560 since there are no secondary carbons. It would therefore be interesting to carry out a more in-depth  
561 study of the structure of the aromatic molecules to confirm the effect of branching on the oxidation  
562 products formed.

#### 563 ***4.1.3. Oxidized products with carbon chain length less than the initial hydrocarbon molecule***

564 In the case of alkane molecules (linear, branched or cyclic), oxidized compounds (2-ketones,  
565 aldehydes and carboxylic acids) with shorter chain lengths than the initial alkane molecule are

566 formed. It is important to note that their formation does not lead to the production of alcohols.  
567 These short-chain oxidized molecules are the result of a different type of mechanism, resulting  
568 from the formation of a ketohydroperoxide (KPH) [7] and subsequent carbon chain cleavage  
569 reactions. These Korcek reactions are also observed in the case of oxidation reactions at  
570 temperatures below 475 °C [73]. It should be noted that the reaction is also an interesting  
571 alternative to explain the formation of short carboxylic acids and aldehydes or ketones [7]. These  
572 mechanisms have been demonstrated in a previous study on n-C<sub>12</sub> [10]. In contrast, for mono- and  
573 di-aromatic molecules, the stability of the benzene rings precludes the possibility of a ring-opening  
574 mechanism. This has already been demonstrated by the small amount of gas obtained. The more  
575 branches a molecule is, the more carbon chain breaking reactions can take place.

#### 576 **4.1.4. Precipitation of polar species**

577 The overall oxidation mechanism of the model molecules studied and the formation of the  
578 associated products in the liquid phase are summarized in Figure 11. All oxidized products are  
579 polar species. It is noteworthy that the formation of SMORS or insoluble deposits do not require the  
580 presence of molecules containing sulphur or nitrogen atoms. The precipitation of polar species can  
581 result from two scenarios: (1) polar species formed during oxidation reactions precipitate due to  
582 the difference in polarity with the hydrocarbon liquid phase [18] ; (2) the polar species formed  
583 react with each other to form SMORS which, due to their weight, precipitate at the bottom of the  
584 crucible.

585 The second scenario can be supported by the mechanism of Adams *et al.* [59], in which the authors,  
586 using DFT calculations, proposed two additional pathways to the SMORS formation mechanism:  
587 (a) a first mechanism in which a quinone can be formed via the decomposition of a tetra peroxide  
588 formed by the reaction of two keto-peroxyl radicals, leading to two reactive hydroxy radicals and

589 singlet oxygen; (b) the second via coupling between the quinone and electron-rich compounds,  
 590 such as indole-type species. The hydroxy radicals then undergo a hydrogen transfer reaction to  
 591 form the quinone and a p-chinole. In the present study, the quinone species involved in mechanism  
 592 (a) were not detected experimentally, so it is unlikely that they were formed under the operating  
 593 conditions used. However, it is conceivable that these products could be formed at  $\Delta P/P_{max} >$   
 594 10% or in the presence of nitrogen or sulphur compounds. The second mechanism (b) is  
 595 conceivable in the presence of heteroatomic species. However, in the present study the  
 596 hydrocarbon species were oxidized alone, without any nitrogen or sulphur species.

597 Another mechanism given in the literature [57,93] for the gel formation involves the presence of  
 598 strong acids (sulphonic acid type) which may play a role in catalysing the formation of the deposits.  
 599 Indeed, the results of the oxidation and analysis of n-C12 IsoB and n-BC in this study revealed a  
 600 significant amount of acidic species, which, although lacking heteroatomic species, may also play  
 601 a catalyzing role.

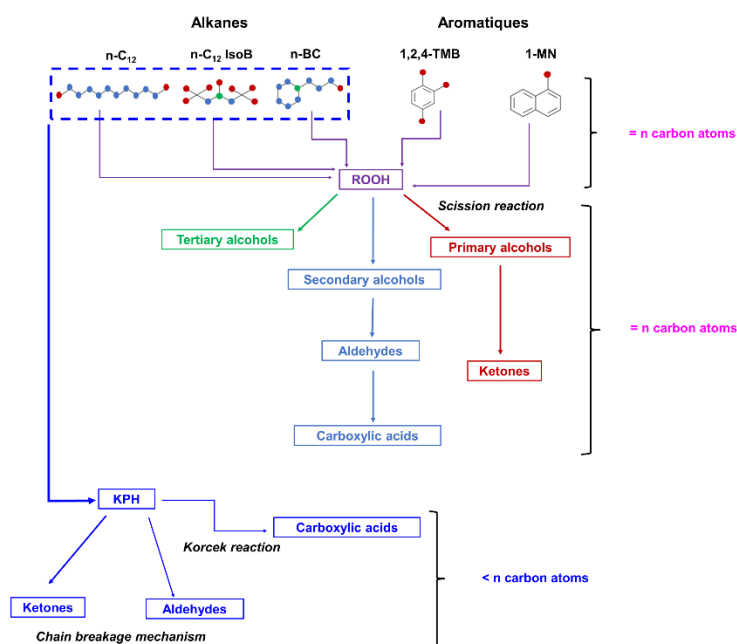


Figure 11 - Global diagram showing the different classes of oxidation products obtained for all model molecules of carbon chain length n

## 602 4.2. Kinetic study

### 603 4.2.1. Global reaction rate constant

604 Based on the same methodology presented in a previous work [10], it was possible to determine  
605 the overall oxidation reaction kinetic constants of the set of model molecules presented in this  
606 study. The mechanism and analysis of Bacha *et al.* [78] were used to determine the overall reaction  
607 rate parameters. However, we have corrected the experimental induction times to be at iso-  
608 conversion of oxygen. Thus, the equation was modified to take into account these new elements,  
609 as shown in Equation 2, where  $\Delta n(O_2)$  and  $\Delta n(RH)$  are the number of moles of oxygen and  
610 hydrocarbon molecules consumed, respectively,  $IP_{corrected}$  is expressed in seconds.

$$\ln \left[ \frac{\Delta n(O_2)}{\Delta n(RH)IP_{corrected}} \right] = - \frac{E_a}{RT} + \ln A \quad \text{Equation 2}$$

611 The corrected induction periods were plotted as a function of 1/T (Figure S.M.7.1.). A linear  
612 regression was used for the determination of  $E_a$  and  $A$  values (Table 4). The rate constants  $k$  of  
613 the oxidation reaction of all model molecules derived from the Arrhenius regression are given in  
614 Table 5 for each test temperature.

615 By comparing the kinetic values obtained for all the model molecules, it is possible to divide them  
616 into 2 categories:

- 617 • alkanes with high activation energy values ( $E_a > 120 \text{ kJ.mol}^{-1}$ ) and high pre-exponential  
618 factors ( $A > 10^{+12}$ );
- 619 • aromatics with slightly lower activation energies ( $E_a < 110 \text{ kJ.mol}^{-1}$ ) and pre-exponential  
620 factors ( $A < 10^{+09}$ ).

Table 4 - Activation energies values ( $E_a$ ) and pre-exponential factors  $A$  for the oxidation

Table 5 - Model molecules oxidation kinetic constants ( $k$ ) determined using Arrhenius regression

reaction of all model molecules ( $\Delta P/P_{max} = 10\%$  et  $T = 140$  à  $160^\circ\text{C}$ )

	Ea (kJ.mol <sup>-1</sup> )	A (s <sup>-1</sup> )
<b>1-MN</b>	80.03	1.25.10 <sup>+06</sup>
<b>1,2,4-TMB</b>	102.73	1.48.10 <sup>+09</sup>
<b>n-BC</b>	131.79	2.36.10 <sup>+13</sup>
<b>n-C<sub>12</sub></b>	128.79	2.86.10 <sup>+12</sup>
<b>n-C<sub>12</sub> IsoB</b>	128.36	1.42.10 <sup>+13</sup>

Temperature (°C)	140	150	160
<b>1-MN</b>	9.65×10 <sup>-05</sup> s <sup>-1</sup>	1.61×10 <sup>-04</sup> s <sup>-1</sup>	2.83×10 <sup>-04</sup> s <sup>-1</sup>
<b>1,2,4-TMB</b>	1.49×10 <sup>-04</sup> s <sup>-1</sup>	3.24×10 <sup>-04</sup> s <sup>-1</sup>	5.91×10 <sup>-04</sup> s <sup>-1</sup>
<b>n-BC</b>	5.23×10 <sup>-04</sup> s <sup>-1</sup>	1.22×10 <sup>-03</sup> s <sup>-1</sup>	3.08×10 <sup>-03</sup> s <sup>-1</sup>
<b>n-C<sub>12</sub></b>	1.49×10 <sup>-04</sup> s <sup>-1</sup>	3.61×10 <sup>-04</sup> s <sup>-1</sup>	8.39×10 <sup>-04</sup> s <sup>-1</sup>
<b>n-C<sub>12</sub> IsoB</b>	8.63×10 <sup>-04</sup> s <sup>-1</sup>	1.92×10 <sup>-03</sup> s <sup>-1</sup>	4.85×10 <sup>-03</sup> s <sup>-1</sup>

621  
 622 Taking into account the activation energy and the pre-exponential factor obtained, it was possible  
 623 to plot ln(A) as a function of ln(Ea). The linear regression allows the Arrhenius parameters to be  
 624 calibrated according to the structure of the molecule oxidized in the temperature range between  
 625 140 and 160 °C. (Figure 12).

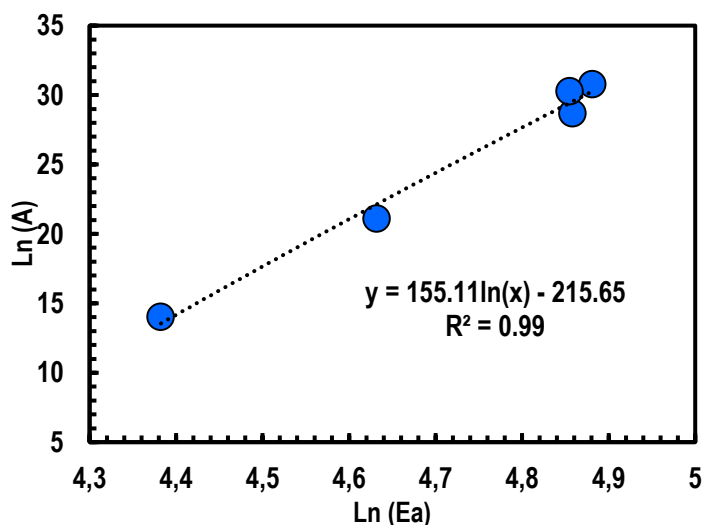


Figure 12 – Experimental calibration model of the Arrhenius parameters of all the model molecules oxidation ( $\Delta P/P_{max}=10\%$ ,  $P_{O_2,i}=700$  kPa,  $T = 140$  to  $160^\circ\text{C}$ )

#### 626 4.2.2. Hydroperoxide dissociation rate constant

627 Two main mechanisms have been proposed in the literature to explain the decomposition of  
 628 hydroperoxides: a self-reaction (Reaction 3) [49,[88] and a homolytic cleavage reaction (Reaction  
 629 4) . Reaction 3 was discarded because the tests were carried out at the very beginning of the

630 autoxidation. This implies a low concentration of hydroperoxides in the solution, thus the  
631 interaction between two molecules is very unlikely. The second is favoured by temperature and  
632 can be considered at low conversion rates.



633 The hydroperoxide dissociation rate constant was determined. Taking into account the qualitative  
634 and quantitative results of the liquid phase of the present study, it can be suggested that the  
635 secondary oxidation products (alcohols, ketones, aldehydes and carboxylic acid) originate from  
636 the formation and decomposition of hydroperoxides [10]. Thus, using the peroxide values  
637 determined experimentally for each temperature, it is possible to establish the evolution of the  
638 hydroperoxide concentration as a function of the duration of the oxidation reaction (Table  
639 S.M.7.2.1).

640 Furthermore, according to the literature [78], the oxygen consumption can be expressed by  
641 Equation 4, where the previously determined kinetic constant  $k$  can be related to Equation 5.  
642 Inserting the kinetic constant  $k$  into Equation 6 and integrating it between  $t = 0$  and  $t = \text{IP}$  gives  
643 the hydroperoxide dissociation rate. The kinetic constant  $k''$  can then be determined from the  
644 experimental data using Equation 7.

645 The kinetic constant of the hydroperoxide dissociation ( $k''$ ) obtained for each temperature tested  
646 is given in Table 7 and  $\ln(k'')$  was plotted as a function of  $1/T$  following the formalism of the  
647 Arrhenius law (Figure S.M.7. 1).

$$-\frac{d[\text{O}_2]}{dt} = k[\text{RO}_2^{\bullet}][\text{RH}] \quad \text{Equation 3}$$

$$\frac{d[\text{RO}_2\text{H}]}{dt} = k'[\text{RO}_2^{\bullet}][\text{RH}] - k''[\text{RO}_2\text{H}] \quad \text{Equation 4}$$

$$k = k' [RO_2^{\bullet}] = A \exp^{-\frac{E_a}{RT}} \quad \text{Equation 5}$$

$$\frac{d[RO_2H]}{dt} = k'[RO_2^{\bullet}][RH] - k''[RO_2H] \quad \text{Equation 6}$$

$$k'' = k \frac{([RH]_{IP_{corrected}} - [RH]_0)}{[RO_2H]_{IP_{corrected}}} \quad \text{Equation 7}$$

648

Table 6- Activation energies values ( $E_a''$ ) and pre-exponential factors  $A''$  of the hydroperoxide dissociation oxidation reaction for all model molecules

( $\Delta P/P_{max} = 10\%$  et  $T = 140$  à  $160^\circ\text{C}$ )

	$E_a''$ (kJ.mol <sup>-1</sup> )	$A''$ (s <sup>-1</sup> )
<b>1-MN</b>	126.50	$2.14.10^{+12}$
<b>1,2,4-TMB</b>	98.58	$5.56.10^{+09}$
<b>n-BC</b>	69.25	$1.05.10^{+06}$
<b>n-C<sub>12</sub></b>	86.80	$2.89.10^{+07}$
<b>n-C<sub>12</sub> IsoB</b>	116.17	$1.78.10^{+12}$

Table 7 - Kinetic constants ( $k''$ ) of the hydroperoxide dissociation during oxidation of model molecules determined using Arrhenius regression estimates from Table 6 and the experimental peroxide values (PV)

Temperature (°C)	140	150	160
<b>1-MN</b>	$2.12 \times 10^{-04} \text{ s}^{-1}$	$5.34 \times 10^{-04} \text{ s}^{-1}$	$1.16 \times 10^{-03} \text{ s}^{-1}$
<b>1,2,4-TMB</b>	$2.04 \times 10^{-03} \text{ s}^{-1}$	$3.29 \times 10^{-03} \text{ s}^{-1}$	$7.70 \times 10^{-03} \text{ s}^{-1}$
<b>n-BC</b>	$1.72 \times 10^{-03} \text{ s}^{-1}$	$3.36 \times 10^{-03} \text{ s}^{-1}$	$4.35 \times 10^{-03} \text{ s}^{-1}$
<b>n-C<sub>12</sub></b>	$3.10 \times 10^{-04} \text{ s}^{-1}$	$5.50 \times 10^{-04} \text{ s}^{-1}$	$9.96 \times 10^{-04} \text{ s}^{-1}$
<b>n-C<sub>12</sub> IsoB</b>	$3.79 \times 10^{-03} \text{ s}^{-1}$	$7.48 \times 10^{-03} \text{ s}^{-1}$	$1.81 \times 10^{-02} \text{ s}^{-1}$

649 By comparing the values of the global constant  $k$  and the dissociation hydroperoxides constant  $k''$

650 (Table 7), it can be seen that  $k < k''$ . This result confirms the experimental results obtained in this

651 study and indicates that the hydroperoxides are consumed very rapidly after their formation. The

652 values of the constant  $k''$  obtained in this work have been compared with those found in the

653 literature (Table 8) but it is difficult to draw conclusions since the latter are mainly average or

654 estimated values for modelling purposes and are already widely scattered.

Table 8. Comparison of the kinetic constants of the hydroperoxide dissociation reaction obtained in the presents study with those reported in the literature.

Literature data	Molecule	A (s <sup>-1</sup> )	Ea (kJ/mol)	Kind of study
<b>Thomas (1955) [89]</b>	Tetralin	$1.3 \times 10^{+11}$	121.3	Experimental
	$\alpha$ -Cumyl	$1.3 \times 10^{+11}$	121.3	
	n-Octyl	$1.0 \times 10^{+10}$	108.8	
	2,2,4-Trimethylpentyl-2	$1.0 \times 10^{+10}$	108.8	
	t-Butyl	$1.2 \times 10^{+15}$	163.2	
	Cyclohexyl	$1.2 \times 10^{+13}$	142.2	
	Decalyl	$8.5 \times 10^{+13}$	133.9	



	Sec-Decyl	$1.0 \times 10^{+11}$	129.7	
<b>Ervin <i>et al.</i>(1998) [90]</b>	Jet A	$1.0 \times 10^{+15}$	154.80	Numerical
<b>Zabarnick (1998) [91] Kuprowicz <i>et al.</i> (2004) [4]</b>	Exxsol D-80	$1.0 \times 10^{+15}$	175.7	Experimental/Numerical, Numerical
<b>Kuprowicz <i>et al.</i> (2007) [30]</b>	Jet A-1, Jet A and JP-8	$1.0 \times 10^{+15}$	163.2	Numerical
<b>West (2011) [74]</b>	Exxsol D-80	$2.0 \times 10^{+8}$	104.6	Numerical
<b>Aminane <i>et al.</i>(2021) [10]</b>	n-C <sub>12</sub>	$2.9 \times 10^{+7}$	86.8	Experimental
<b>Alborzi <i>et al.</i>(2021) [92]</b>	n-C <sub>12</sub>	$5 \times 10^{13}$	138.1	Numerical

## 655 5 CONCLUSION

656 This study demonstrates the impact of the structure of the model molecules (n-alkane, i-alkane,  
657 cyclo-alkane, mono-aromatic and di-aromatic) present in the jet fuel during their autoxidation  
658 process in the liquid phase, using the PetroOXY apparatus. The experimental conditions were  
659 chosen at low advancement values ( $\Delta P/P_{\max} = 2-10\%$ ) in order to gain a better understanding of  
660 the initial stages of the reaction.

661 The robust experimental strategy employed allowed to qualitatively and quantitatively monitor the  
662 consumption of the reactants (oxygen and hydrocarbons) as well as characterizing their  
663 degradation products. Reagent monitoring showed that oxygen consumption was always higher  
664 than that of the parent hydrocarbons, suggesting that oxygen is used in two types of competitive  
665 reactions: with the parent hydrocarbon and with the oxidation products. Although the overall  
666 behavior of oxygen consumption is similar for all alkane molecules, for aromatics the behavior  
667 varies according to their structure. The degree of branching of a molecule also affects its reactivity  
668 and the products formed. This is an important milestone: the nature and structure of the molecule  
669 influences its oxidation rate and mechanism.

670 The structure-reactivity aspect was also highlighted by the identification and quantification of the  
671 oxidation products in both the gas and liquid phases. The quantity of gaseous products is very small  
672 and linked to the breaking of the carbon chains of the hydrocarbons. CO<sub>2</sub> is the main product  
673 formed and its quantity increases much more than the other molecules. The amount of gas formed  
674 depends on the nature of the molecule and its chemical structure: the more branched a molecule  
675 is, the more the carbon chain breaking reactions occur. In the liquid phase, the same oxidation  
676 products are detected for a given molecule, regardless of the progress of the reaction and  
677 temperature. The elimination of the hydrogen atom to form the radical that reacts with the oxygen  
678 can occur anywhere in the molecule except at the aromatic ring. This leads to the formation of all  
679 possible hydroperoxides isomers. The proportions of the products (primary, secondary and tertiary  
680 alcohols, ketones and acids) are therefore directly dependent on this. Finally, a gel precursor  
681 deposit was obtained after oxidation of the molecules, highlighting a potential precipitation of  
682 polar species due to the difference in polarity with hydrocarbon molecules.

683 The results obtained at different temperatures were used to calculate the overall reaction constant  
684 and the dissociation constant of hydroperoxide. They also enabled to determine the consumption  
685 rates of the reactants, to follow the formation of the products over time, to confirm the choice of a  
686 mechanism and to determine the kinetic constants. These data are valuable to further model the  
687 autoxidation of the model molecules as a function of time, with the aim of reconciling the different  
688 experimental and simulation curves.

689 To gain a better insight of the degradation of a jet fuel, the next steps will also to (1) use the same  
690 methodology in the presence of sulphur or nitrogen species to evaluate their impact on deposit  
691 formation and (2) to mix all the families of molecules studied individually here in the proportions  
692 of a SAF to get closer to a surrogate. In this way, using the same approach and associating other

693 characterization techniques, such as GCxGC, it would be possible to determine the kinetic  
694 parameters necessary to calibrate the numerical simulation models of deposits formation.  
695 Moreover, it would be relevant to experimentally confirm the data obtained by DFT, using the  
696 same methodology as proposed in this study.

697

## 698 REFERENCES

- 699 [1] Heneghan S. P., Zabarnick S., Oxidation of jet fuels and the formation of Deposits, *Fuel*, 1994, 73, 1, 35-43.
- 700 [2] Pradelle, F., Braga, S.L., Martins, A.R.F.A., Turkovics, F., Pradelle, R.N.C., Gum formation in gasoline and its blends: a review,  
701 *Energy Fuels*, 2015, 29, 7753– 7770.
- 702 [3] Zabarnick, S., Chemical kinetic modeling of jet fuel autoxidation and antioxidant chemistry. *Ind. Eng. Chem. Res.* 1993, 32,  
703 1012–1017.
- 704 [4] Kuprowicz N. J., Ervin J.S. , Zabarnick S., Modeling the liquid-phase oxidation of hydrocarbons over a range of temperatures  
705 and dissolved oxygen concentrations with pseudo-detailed chemical kinetics, *Fuel*, 2004, 83 1795– 1801.
- 706 [5] Garcia-Ochoa F., Romero A., Querol J., Modeling of the Thermal n-Octane Oxidation in the Liquid Phase, *Ind. Eng. Chem.*  
707 *Res.*, 1989, 28, 43-48.
- 708 [6] Webster, R.L., Evans, D.J., Marriott, P.J., Multidimensional gas chromatographic analysis of low-temperature oxidized jet  
709 fuels: formation of alkyldihydrofuranones, *Energy Fuels*, 2015, 29, 2067–2073.
- 710 [7] Jalan A, Alecu IM, Meana-Pañeda R, Aguilera-Iparraguirre J, Yang KR, Merchant SS, et al. New pathways for formation of  
711 acids and carbonyl products in low- temperature oxidation: the korcek decomposition of  $\gamma$ -keto hydroperoxides. *J. Am. Chem.*  
712 *Soc.* 2013;135(30):11100–14.
- 713 [8] Marteau C, Ruyffelaere F, Aubry J-M, Penverne C, Favier D, Nardello-Rataj V. Oxidative degradation of fragrant aldehydes,  
714 Autoxidation by molecular oxygen. *Tetrahedron*, 2013,69(10),2268–75.
- 715 [9] Webster, R.L., Rawson, P.M., Kulsing, C., Evans, D.J., Marriott, P.J., Investigation of the thermal oxidation of conventional  
716 and alternate aviation fuels with comprehensive two-dimensional gas chromatography accurate mass quadrupole time-of-flight  
717 mass spectrometry, *Energy Fuels*, 2017, 31, 4886–4894.
- 718 [10] Aminane S., Sicard M., Melliti Y., Ser F., Lorette Sicard L., Experimental study of the kinetics of degradation of n-dodecane  
719 under thermo-oxidative stress at low temperature and mechanism inferred, *Fuel*, 2021, 307,121669.
- 720 [11] Christison, K.M., Lorenz, R.M., Xue, L., Sparkman, O.D., Exploring the molecular origin of jet fuel thermal oxidative  
721 instability through statistical analysis of mass spectral data, *Energy Fuels*, 2019, 33, 830–836.
- 722 [12] Hardy, D.R., Wechter, M.A., Insoluble sediment formation in middle-distillate diesel fuel: the role of soluble macromolecular  
723 oxidatively reactive species. *Energy Fuels*, 1990, 4 (3), 270–274.
- 724 [13] Hardy, D.R., Wechter, M.A., Characterization of soluble macromolecular oxidatively reactive species (SMORS) from middle  
725 distillate diesel fuels: their origin and role in instability, *Energy Fuels*, 1994, 8, 782–787.

- 726 [14] Beaver, B., Gao, L., Burgess-Clifford, C., Sobkowiak, M., On the mechanisms of formation of thermal oxidative deposits in  
727 jet fuels. Are unified mechanisms possible for both storage and thermal oxidative deposit formation for middle distillate fuels,  
728 *Energy Fuels*, 2005, 19, 1574–1579.
- 729 [15] Commodo, M., Fabris, I., Groth, C.P.T., Gülder, Ö.L., Analysis of aviation fuel thermal oxidative stability by electrospray  
730 ionization mass spectrometry (ESI–MS), *Energy Fuels*, 2011, 25, 2142–2150.
- 731 [16] Commodo, M., Fabris, I., Wong, O., Groth, C.P.T., Gülder, Ö.L., Threedimensional fluorescence spectra of thermally stressed  
732 commercial Jet A-1 aviation fuel in the autoxidative regime, *Energy Fuels*, 2012, 26, 2191–2197.
- 733 [17] Commodo, M., Wong, O., Fabris, I., Groth, C.P.T., Gülder, Ö.L., Spectroscopic study of aviation jet fuel thermal oxidative  
734 stability, *Energy Fuels*, 2010, 24, 6437–6441.
- 735 [18] Alves-Fortunato M., Ayoub E., Bacha K., Dalmazzone C., Fatty Acids Methyl Esters (FAME) autoxidation: New insights on  
736 insoluble deposit formation process in biofuels, *Fuel*, 2020, 268, 117074.
- 737 [19] Kabana, C.G., Botha, S., Schmucker, C., Woolard, C., Beaver, B., Oxidative stability of middle distillate fuels. Part 1:  
738 exploring the soluble macromolecular oxidatively reactive species (SMORS) mechanism with jet fuels, *Energy Fuels*, 2011,  
739 25,(11) 5145–5157.
- 740 [20] Aksoy, P., Gül, Ö., Cetiner, R., Fonseca, D.A., Sobkowiak, M., Falcone-Miller, S., Miller, B.G., Beaver, B., Insight into the  
741 mechanisms of middle distillate fuel oxidative degradation. Part 2: on the relationship between jet fuel thermal oxidative  
742 deposit, soluble macromolecular oxidatively reactive species, and smoke point, *Energy Fuels*, 2009, 23, 2047–2051.
- 743 [21] Jia, T., Pan, L., Gong, S., Xie, J., Wang, X., Fang, Y., Zou, J.-J., Zhang, X., Mechanistic insights into the thermal deposition  
744 of highly thermal-stable jet fuel, *Fuel*, 2020, 276, 118100.
- 745 [22] Jones E. G., Balster W.J., Phenomenological Study of the Formation of Insolubles in a Jet-A Fuel, *Energy & Fuels* 1993, 7,  
746 968-977.
- 747 [23] Chatelain K., Nicolle A., Ben Amara A., Catoire L., Starck L., Wide Range Experimental and Kinetic Modeling Study of  
748 Chain Length Impact on n-Alkanes Autoxidation, *Energy Fuels*, 2016, 30, 1294–1303.
- 749 [24] Zhao, L., Zhang, X., Pan, L., Liu, J., Storage period prediction and metal compatibility of endothermic hydrocarbon fuels,  
750 *Fuel*, 2018, 233, 1–9.
- 751 [25] Sarnecki, J., Gawron, B., Gła b, J., Hydroperoxides formation in jet fuels coming from different production processes in  
752 simulated fuel system of modern aircraft, *J. KONBiN*, 2017, 43, 277–299.
- 753 [26] Edwards, T., Cracking and deposition behavior of supercritical hydrocarbon aviation fuels, *Combust. Sci. Technol.*, 2006,  
754 178, 307–334.
- 755 [27] DeWitt M.J., West Z., Zabarnick S., Shafer L., Striebich R., Edwards T., Effect of addition of aromatics on the thermal-  
756 oxidative stability of alternative aviation fuel, IASH 2013, the 13th International Symposium on Stability, Handling, and Use  
757 of Liquid Fuels, Rhodes, Greece, 6-10 October, 2013.
- 758 [28] Ervin, J.S., Ward, T.A., Williams, T.F., Bento, J., Surface deposition within treated and untreated stainless steel tubes resulting  
759 from thermal-oxidative and pyrolytic degradation of jet fuel, *Energy Fuels*, 2003, 17, 577–586.
- 760 [29] Tao Z., Fu Y., Xu G., Deng H., Jia Z., Experimental study on influences of physical factors to supercritical RP-3 surface and  
761 liquid-space thermal oxidation coking, *Energy Fuels*, 2014, 28, 6098–6106.
- 762 [30] Kuprowicz, N. J., Zabarnick, S. West, Z. J., Ervin J. S. Use of Measured Species Class Concentrations with Chemical Kinetic  
763 Modeling for the Prediction of Autoxidation and Deposition of Jet Fuels, *Energy & Fuels* 2007, 21, 530-544.
- 764 [31] Venkataraman, R., Eser, S., Characterization of solid deposits formed from short durations of jet fuel degradation:  
765 carbonaceous solids. *Ind. Eng. Chem. Res.*, 2008, 47, 9337–9350.

- 766 [32] Velkavrh, I., Palamarciuc, I., Galus D.G., Diem, A., Brenner, J., Gabler, C., Mellor, B., Ratoi, M., Formation of surface  
767 deposits on steel and titanium aviation fuel tubes under real operating conditions. *ACS Omega*, 2019, 4, 8255–8273.
- 768 [33] Fu, Y., Xu, G., Wen, J., Huang, H., Thermal oxidation coking of aviation kerosene RP-3 at supercritical pressure in helical  
769 tubes, *Appl. Therm. Eng.* 2018, 128, 1186–1195.
- 770 [34] Jiang, H., Ervin, J.S., Zabarnick, S., West, Z., Effects of flow passage expansion or contraction on jet-fuel surface deposition.  
771 *J. Propuls. Power*, 2012, 28, 694–706.
- 772 [35] Han Z., Zhou W., Zan H., Jia Z., Martynenko S., Yanovskiy L., Numerical investigation on influences of inlet flow pattern on  
773 RP-3 thermal oxidation deposition, *Fuel*, 2021, 303, 121314.
- 774 [36] Sander Z.H., West Z.J., Ervin J.S., Zabarnick S., Experimental and Modeling Studies of Heat Transfer, Fluid Dynamics, and  
775 Autoxidation Chemistry in the Jet Fuel Thermal Oxidation Tester (JFTOT), *Energy Fuels*, 2015, 29, 7036-7047.
- 776 [37] Beaver, B.D., Clifford, C.B., Fedak, M.G., Gao, L., Iyer, P.S., Sobkowiak, M., High heat sink jet fuels - Part 1. Development  
777 of potential oxidative and pyrolytic additives for JP-8, *Energy Fuels*, 2006, 20, 1639–1646.
- 778 [38] Pei X-Y, Hou L-Y., Effect of dissolved oxygen concentration on coke deposition of kerosene, *Fuel Processing Technology*,  
779 2016, 142, 86–91.
- 780 [39] Beaver, B., Gao, L., Burgess-Clifford, C., Sobkowiak, M., On the mechanisms of formation of thermal oxidative deposits in  
781 jet fuels. Are unified mechanisms possible for both storage and thermal oxidative deposit formation for middle distillate fuels,  
782 *Energy Fuels*, 2005, 19, 1574–1579.
- 783 [40] Adams, R.K., Zabarnick, S., West, Z.J., Striebich, R.C., Johnson, D.W., Chemical analysis of jet fuel polar, heteroatomic  
784 species via high-performance liquid chromatography with electrospray ionization–mass spectrometric detection, *Energy Fuels*,  
785 2013, 27, 2390–2398.
- 786 [41] Zabarnick, S., West, Z.J., Shafer, L.M., Mueller, S.S., Striebich, R.C., Wrzesinski, P.J., Studies of the role of heteroatomic  
787 species in jet fuel thermal stability: model fuel mixtures and real fuels, *Energy Fuels*, 2019, 33, 8557–8565.
- 788 [42] Link, D.D., Baltrus, J.P., Zandhuis, P., Isolation and identification of nitrogen species in jet fuel and diesel fuel, *Energy Fuels*,  
789 2007, 21, 1575–1581.
- 790 [43] Balster, L.M., Zabarnick, S., Striebich, R.C., Shafer, L.M., West, Z.J., Analysis of polar species in jet fuel and determination  
791 of their role in autoxidative deposit formation, *Energy Fuels*, 2006, 20, 2564–2571.
- 792 [44] Sobkowiak, M., Griffith, J.M., Wang, B., Beaver, B., Insight into the mechanisms of middle distillate fuel oxidative  
793 degradation. Part 1: on the role of phenol, indole, and carbazole derivatives in the thermal oxidative stability of Fischer-  
794 Tropsch/petroleum jet fuel blends, *Energy Fuels*, 2009, 23, 2041–2046.
- 795 [45] Epping, R., Kerkering, S., Andersson, J.T., Influence of different compound classes on the formation of sediments in fossil  
796 fuels during aging, *Energy Fuels*, 2014, 28, 5649–5656.
- 797 [46] Rawson, P.M., Webster, R.L., Evans, D., Abanteriba, S., Contribution of sulfur compounds to deposit formation in jet fuels at  
798 140 °C using a quartz crystal microbalance technique, *Fuel*, 2018, 231, 1–7.
- 799 [47] AlGhani, M.J.A., Comparative study in evaluating the antioxidation efficiency for native type’s antioxidants extracted from  
800 crude oil with the synthesized class, *World Acad. Sci. Eng. Technol.*, 2016, 10, 1345–1348.
- 801 [48] Hazlett, R., Distillate Fuel Insolubles: Formation Conditions and Characterization, *Energy & Fuels*, 1991, 5, 269-273.
- 802 [49] Alborzi, E., Gadsby, P., Mohammed, S. I., Sheikhsari, A., Dwyer, M., Meijer, A., Blakey, S., Pourkashanian, M.,  
803 Comparative Study of the Effect of Fuel Deoxygenation and Polar Species Removal on Jet Fuel Surface Deposition, *Energy &*  
804 *Fuels*, 2019, 33, 1825-1836.

- 805 [50] Waynick, J.A., The development and use of metal deactivators in the petroleum industry: a review, *Energy Fuels*, 2001, 15,  
806 1325–1340.
- 807 [51] West, Z.J., Adams, R.K., Zabarnick, S., Homogeneous catalysis of liquid-phase hydroperoxide decomposition in  
808 hydrocarbons, *Energy Fuels*, 2011, 25, 897–904.
- 809 [52] Antonio, E.N., Wicking, C., Filip, S., Ryan, M.P., Heutz, S., Role of iron speciation in oxidation and deposition at the  
810 hexadecane-iron interface, *ACS Appl. Mater. Interfaces*. 2020, 12, 19140–19152.
- 811 [53] Pfaendtner J., Broadbelt L.J., Elucidation of structure–reactivity relationships in hindered phenols via quantum chemistry and  
812 transition state theory, *Chemical Engineering Science*, 2007, 62, 5232 - 5239.
- 813 [54] Dinkov R., Hristov G., Stratiev D., Boynova Aldayri V, Effect of commercially available antioxidants over biodiesel/diesel  
814 blends stability, *Fuel*, 2009, 88, 732–737.
- 815 [55] Parks, C., Alborzi, E., Blakey, S., Meijer, A., Pourkashanian, M., Density Functional Theory Calculations on Copper-Mediated  
816 Peroxide Decomposition Reactions: Implications for Jet Fuel Autoxidation, *Energy Fuels* 2020, 34, 6, 7439–7447.
- 817 [56] Zabarnick, S., Phelps D., Density Functional Theory Calculations of the Energetics and Kinetics of Jet Fuel Autoxidation  
818 Reactions, *Energy Fuels*, 2006, 20, 2, 488–497.
- 819 [57] Parks C., Meijer, A., Blakey, S., Alborzi, E., Pourkashanian, M., Computational studies on the reactions of thiols, sulfides and  
820 disulfides with hydroperoxides. Relevance for jet fuel autoxidation, *Fuel*, 2022, 316, 123326.
- 821 [58] Alborzi, E., Dweyer, M., Parks, C., Sheikhsari, A., Mielczarek, D., Zanganeh, M., Meijer, A., Blakey, S., Pourkashanian,  
822 M., Construction of a reduced chemical kinetic mechanism for autoxidation of n-paraffinic solvent – A model for aviation fuel,  
823 *Fuel*, 2021, 294, 120170.
- 824 [59] Adams, C., Alborzi, E., Meijer, A., Hughes, K., Mechanistic investigation into the formation of insolubles in bulk fuel jet fuel  
825 using quantum chemical and experimental techniques, *Fuel*, 2023, 334, 126202
- 826 [60] ASTM D7525 – 14 - *Standard Test Method for Oxidation Stability of Spark Ignition Fuel—Rapid Small Scale Oxidation Test*  
827 (*RSSOT*), ASTM International, West Conshohocken, PA, 2019.
- 828 [61] ASTM D7545 - 09 *Standard Test Method for Oxidation Stability of Middle Distillate Fuels—Rapid Small Scale Oxidation*  
829 *Test (RSSOT)* , ASTM International, West Conshohocken, PA, 2009.
- 830 [62] EN 16091 - *Liquid petroleum products. Middle distillates and fatty acid methyl ester (FAME) fuels and blends. Determination*  
831 *of oxidation stability by rapid small scale oxidation method*, European Committee for Standardization, Berlin, 2011.
- 832 [63] Machado Y.L, Teles U.M., Neto A.A. D., Dantas T.N.C., Fonseca J.L.C., *Determination of antioxidant depletion kinetics*  
833 *using ASTM D 7545 as the accelerated oxidation method*, *Fuel*, 2013, 112, 172-177.
- 834 [64] Ben Amara A., Kaoubi S., Starck L., *Toward an optimal formulation of alternative jet fuels: Enhanced oxidation and thermal*  
835 *stability by the addition of cyclic molecules*, *Fuel*, 2016, 173, 98-105.
- 836 [65] Sicard, M.; Boulicault, J.; Coulon, K.; Thomasset, C.; Ancelle, J.; Raepsaet, B.; and Ser, F. Oxidation stability of jet fuel  
837 model molecules evaluated by rapid small scale oxidation tests, The 13th International Conference on Stability, Handling and  
838 Use of Liquid Fuels, IASH 2013.
- 839 [66] West ZJ, Zabarnick S, Striebich RC. Determination of hydroperoxides in jet fuel via reaction with triphenylphosphine. *Ind.*  
840 *Eng. Chem. Res.* 2005;44(10):3377–83.
- 841 [67] Wiklund P, Karlsson C, Levin M. Determination of hydroperoxide content in complex hydrocarbon mixtures by gas  
842 chromatography/mass spectrometry. *Anal Sci* 2009;25(3):431–6.

- 843 [68] ASTM D 3703-13 - Standard Test Method for Hydroperoxide Number of Aviation Turbine Fuels, Gasoline and Diesel Fuels,  
844 ASTM International: West Conshohocken, PA, 2013.
- 845 [69] Pullen J, Saeed K. An overview of biodiesel oxidation stability. *Renew Sustain Energy Rev* 2012;16 (8),5924–50.
- 846 [70] ASTM D3242-08 - Standard Test Method for Acidity in Aviation Turbine Fuel., ASTM International: West Conshohocken,  
847 PA, 2008.
- 848 [71] Reddy K. T., Cernansky N. P., Modified Reaction Mechanism of Aerated n –Dodecane Liquid Flowing over Heated Metal  
849 Tubes, *Energy & Fuels*, 1988, 2, 205-213.
- 850 [72] Blin-Simiand N., Jorand F., Sahetchian K., Hydroperoxides With Zero, One, Two or More Carbonyl Groups Formed During  
851 the Oxidation of N-Dodecane, *Combustion and Flame*, 2001, 126, 1524–1532.
- 852 [73] Sarathy SM, Westbrook CK, Mehl M, Pitz WJ, Togbe C, Dagaut P, et al. Comprehensive chemical kinetic modeling of the  
853 oxidation of 2-methylalkanes from C7 to C20. *Combust Flame* 2011;158(12):2338–57.
- 854 [74] West, Dissertation, Studies of Jet fuel autoxidation chemistry: Catalytic hydroperoxydes decomposition & High heat flux  
855 effects, The School of Engineering of the University of Dayton, 2011.
- 856 [75] Ben Amara A, Nicolle A, Alves-Fortunato M, Jeuland N. Toward predictive modeling of petroleum and biobased fuel stability:  
857 kinetics of methyl oleate/n-dodecane autoxidation. *Energy Fuels* 2013;27(10):6125–33.
- 858 [76] Chatelain K, Nicolle A, Ben AA, Catoire L, Starck L. Wide range experimental and kinetic modeling study of chain length  
859 impact on n-alkanes autoxidation. *Energy Fuels* 2016;30:1294–303.
- 860 [77] Chatelain K, Nicolle A, Ben Amara A, Starck L, Catoire L. Structure– reactivity relationships in fuel stability: experimental  
861 and kinetic modeling study of isoparaffin autoxidation. *Energy Fuels* 2018;32(9):9415–26.
- 862 [78] Bacha K, Ben-Amara A, Vannier A, Alves-Fortunato M, Nardin M. Oxidation stability of diesel/biodiesel fuels measured by  
863 a petrooxy device and characterization of oxidation products. *Energy Fuels* 2015;29(7):4345–55.
- 864 [79] Gürsoy T., ATR-FTIR Analyses for a series transactions of potato plant wastes performed in order to prepare composite filling,  
865 International Engineering and Natural Sciences Conference (IENSC 2018), Nov. 2018
- 866 [80] Copicova J., Synytsya A., Cerna M., Kaasova J., Novotna M., Application of FT-IR Spectroscopy in Detection of Food  
867 Hydrocolloids in confectionery Jellies and Food Supplements, *Czech J.Food Sci.*, 2001, 19 (2), 51-56
- 868 [81] Dordevic M., Stankovic M.N., Dordevic M.G., Krstic S., Pavlovic M.A., Radivojevic A.R., FTIR Spectroscopic  
869 characterization of bituminous limestone maganik mountain ,*Studia UBB Chemia, Montenegro, LVII*, 4, 2012 (p. 39-54)
- 870 [82] Furutachi H., Hashimoto K., Nagatomo S., Endo T., Fujinami S., Watanabe Y., Kitagawa T., Suzuki M., Reversible O-O  
871 Bond Cleavage and Formation of a Peroxo Moiety of a Peroxocarbonate Ligand Mediated by an Iron(III) Complex, *Journal*  
872 *of the American Chemical Society*, 2005, 127, 4550-4551
- 873 [83] Socrates G., *Infrared and Raman Characteristic Group Frequencies: Tables and Charts*, 3rd Edition, (2004, ISBN: 978-0-  
874 470-09307-8 )
- 875 [84] Larkin P.J. , *IR and Raman Spectroscopy. Principles and Spectral Interpretation* , 2011, Elsevier, ISBN: 978-0-12-386984-5
- 876 [85] Lecomte J., Spectres d’absorption infrarouges d’éthers-sels organiques aliphatiques. Modes de vibration et structure du  
877 groupement carboxyle dans ces composés, *Le Journal de Physique et le Radium*, 1942, 3, 8 (11), 193 -200
- 878 [86] Raynaud C., *Spectroscopie et Réactivité en Chimie Organométallique : Quelques Apports de la Chimie Théorique*,  
879 *Habilitation à diriger des recherches*, 2014, Université Pierre et Marie Curie, Sorbonne Universités

- 880 [87] Gernigon S., Étude de la stabilité à l'oxydation des carburants liquides hydrocarbonées, Influence et comportement des  
881 antioxydants, Thèse de doctorat, 2010, Université Paris Diderot, ONERA
- 882 [88] Bateman L., Hughes H., Morris A. L. , Hydroperoxide Decomposition Hydroperoxide Decomposition In Relation To The  
883 Initiation Of Radical Chain Reactions, Discuss. Faraday Soc., 1953, 14
- 884 [89] Thomas, J.R. The Thermal Decomposition of Alkyl Hydroperoxides. J. Am. Chem. Soc., 1955, 77, 246-248.
- 885 [90] Ervin J. S., Williams T. F. , Dissolved Oxygen Concentration and Jet Fuel Deposition, Ind. Eng. Chem. Res. 1996, 35, 899-  
886 904.
- 887 [91] Zabarnick S., Pseudo-Detailed Chemical Kinetic Modeling of Antioxidant Chemistry for Jet Fuel Applications, Energy &  
888 Fuels, 1998, 12, 547-553.
- 889 [92] Alborzi E., Dwyer M.R., Parks C.M., Sheikhsari A., Mielczarek D.C., Zanganeh M., Meijer A. J.H.M. , G. Blakey S.G.,  
890 Pourkashanian M., Construction of a reduced chemical kinetic mechanism for autoxidation of n-paraffinic solvent – A model  
891 for aviation fuel, Fuel , 2021, 294, 120170.
- 892 [93] Hazlett R.N., Schreifels J.A., Stalick W.M., Morris R.E., Mushrush G.W. Distillate fuel insolubles: Formation conditions  
893 and characterization, Energy Fuels, 1991, 5 (2) , 269-273
- 894